# Development of a Variable-Friction Shoe Surface Mechanism

Michael Elliot King

***Abstract*—In order to treat and prevent accidents caused by balance-failure and friction-induced falls, a proper simulation environment is needed so users can be exposed to controlled slip conditions and trained to improve balance. This report covers the design of a mechanism that fits in the sole of a shoe and can dynamically actuate a brake that varies the coefficient of friction between the shoe and the walking surface. As it is vital to replicate a realistic sense of walking and slipping, the mechanism must be non-obtrusive and high-fidelity, and able to simulate a continuous range of surfaces, such as ice, wet grass, sand, or snow.**

## I. Introduction

The *Shared Reality Lab of the McGill Centre for Intelligent Machines*, under the supervision of Professor Jeremy Cooperstock, has been involved in the field of natural interactive walking for several years and published studies on different variable friction surfaces [1], [2]. The idea of developing a variable-friction device for friction-controlled walking comes from these studies, and their research provides a basis for the design of a shoe mechanism with a dynamically controlled friction coefficient.

### A. Background

In the following explanation of the motivations behind the proposed work, the draft manuscript from a previous study is paraphrased, which includes some references to statistics concerning balance failures [1]. In the age group of those 65 years and older, falls are the cause of 88% of injuries [3], and can lead to their loss of independence and even death. It has been shown in Canada [3], the United States [4], China [5], and Finland [6], that one in three of those this age will fall once a year. Dealing with these injuries involves preventative measures, such as studying the way people walk and react to walking surfaces, as well as rehabilitation, like balance and mobility training. For rehabilitation training, simulated environments must be created to properly imitate the slip environments that cause people to fall. This requires the control of such an environment, by creating a surface with a dynamic coefficient of friction, similar to a natural environment with real obstacles.

Designing a variable-friction walking surface has the potential to be useful in clinical or rehabilitation applications to simulate low-friction induced accidents. Research has been completed already to create a floor surface with very low coefficients of static friction, but has proven to be limited in supported footwear and in simulating natural walking patterns. The technology and expense behind creating a useful walking surface is also a limiting factor. By developing a shoe with the capabilities of varying the friction at the contact surface, more possibilities exist for floor types, and simulating natural walking becomes easier. The main challenge remains to be implementing the proper technology into the sole of a shoe, hence the inspiration for such a project.

## II. Research

### A. Related Work

Based on Coulomb's model of friction, dry friction is the tangential force that resists motion to sliding between two dry, solid materials in contact with each other. Friction force is equal to the normal force on the surface times a coefficient that describes the resistance to sliding motion for that material, known as the coefficient of friction (CoF). The coefficient of static friction between two materials, $\mu_S$, can be empirically determined by taking the tangent of the angle at which one material begins to slip over the other. When walking, the surface of a shoe relies on the reaction force of friction, to resist the tangential force delivered by the user of the shoe, in order to be propelled forward.

With the objective of modifying the friction coefficient from high to low, between a shoe and floor surface, the challenge lies in achieving low friction. To lower the coefficient of friction between two materials, one method is to modify the type of friction. Lubrication introduces a fluid and changes the contact to wet friction, mechanisms like bearings initiate rolling friction, and generating vibrations relies on kinetic friction. Each of these types of friction involves slightly different principles from static dry friction, but all have a lower CoF. Some of these methods were explored and are discussed in further detail in Millet et al [1]. These include a floor surface with rolling ball transfer units, a vibrating floor surface, a floor with sharp protruding pins, and a shoe with vibrating pads in the sole.

The floor surface prototypes both proved to be costly and difficult to implement, because of the need to cover a large area for a user to walk. Additionally, the ball transfer units interfered with natural walking patterns, and the mechanical feasibility of the protruding pins prototype was limited. When attempting to put the variable-friction mechanism into the shoe, with the vibrating pads model, the motion of the pads resulted in an overall translation of the shoe, which impedes natural walking.

Another method, which operates on the principle of dry friction, is to use materials which are naturally slippery. A device has yet to be developed that employs dry friction between the ground and two different "rubbing areas," in

the sole of a shoe, and is dynamically controlled. Through a combination of high and low friction materials, that could be activated by a motor, a large range of friction coefficients can be achieved. This concept is investigated below, through the design and implementation of a mechanism to achieve this behavior.

### B. Calculations

Variable friction means simulating many different levels of static friction on a spectrum that ranges from normal contact friction between a rubber sole and the ground (about $\mu = 0.3$) to slipping on something as slippery as ice (about $\mu = 0.06$) [7]. As Millet showed, polytetrafluoroethylene (PTFE) is the best slip surface as it has a self contact coefficient, $\mu_S$, of about 0.05, which works well to simulate ice. For a high friction surface, gum rubber has an ideal $\mu_S$ against PTFE of 0.55-0.65 [1].

Within this range, it is important to define the necessary step size needed to achieve a smooth, varying friction, based on the needs of the simulation. We have chosen to use ten different variations of friction in the range of $\mu = 0.06$ and $0.3$, with finer resolution as friction approaches the slip condition (Table I).

| | $\mu$ |
|---|---|
| 1 | 0.06 |
| 2 | 0.07 |
| 3 | 0.08 |
| 4 | 0.09 |
| 5 | 0.10 |
| 6 | 0.12 |
| 7 | 0.14 |
| 8 | 0.16 |
| 9 | 0.20 |
| 10 | 0.30 |

TABLE I
DESIRED COEFFICIENTS OF FRICTION (COF)

To achieve these levels of friction, we rely on the mechanical properties of a deformable material to vary the distribution of load between the high and low friction surfaces. Part of the high friction surface, from now on referred to as the "brake," must be a deformable foam, with a linear elastic modulus. When the brake is extended, the deformable material compresses until the surface is at an equal height with the low-friction material, and the force applied through the brake is proportional to the amount of compression. By increasing the height of the brake, the force through the brake increases, and as the coefficient of friction is proportional to the normal force, it increases as well.

Equation 1 shows the friction force on one braking pad, the friction force that is ultimately being controlled.

$$F^{\text{brake}}_{\text{friction}} = \mu_{\text{rubber}} F^{\text{brake}}_{\text{human}} \tag{1}$$

The force from the human causes a strain proportional to the Elastic Modulus of the brake material, causing the brake to deform.

$$F^{\text{brake}}_{\text{human}} = \frac{E_{\text{brake}} S_{\text{brake}} \Delta L}{L} \tag{2}$$

When the deformation, $\Delta L$, is limited to the length of protrusion of the active brake mechanism, only the $F^{\text{brake}}_{\text{human}}$ that satisfies this equation will be transmitted through the brake. The rest of the force of the human will be supported by the slip material around the edges, and it is this relationship between the force on the brake and the slip surface that varies the friction. This is shown in Equation 3 given by Millet et al [1].

$$F_{\text{human}} = F_{\text{low friction}} + F_{\text{high friction}} \tag{3}$$

Equation 2 can be rewritten more generally as

$$F_{\text{high friction}} = E_{\text{elastic}} S_{\text{elastic}} \varepsilon_{\text{elastic}} \tag{4}$$

and combined with Equations 3 and 1 to give the relationship between the coefficients of friction, and how the effective CoF is achieved (Equation 5).

$$\mu_{\text{effective}} = \mu_{\text{low}} + (\mu_{\text{high}} - \mu_{\text{low}}) \frac{E_{\text{elastic}} S_{\text{elastic}} \varepsilon_{\text{elastic}}}{F_{\text{human}}} \tag{5}$$

where $F_{\text{human}}$ is the vertical force applied on the shoe, $F_{\text{low friction}}$ is the normal force on the low friction surface, $F_{\text{high friction}}$ is the normal force on the high friction surface, $E_{\text{elastic}}$ is the Young's Modulus of the elastic element, $\varepsilon_{\text{elastic}}$ is the controlled deformation of the elastic material, $S_{\text{elastic}}$ is the surface area of the high friction surface, and $\mu_{\text{low}}$ and $\mu_{\text{high}}$ are the respective coefficients of friction.

Using Equation (5), taking $S_{\text{elastic}}$ and $F_{\text{human}}$ to be constant, and only considering $E_{\text{elastic}}$ in the linear region, we can solve for $\varepsilon_{\text{elastic}}$ or $\Delta L$ for each desired $\mu_{\text{effective}}$. From this deformation, the translation needed to vary the friction by the desired amount is known.

To verify that the desired friction can be achieved, we can compare the abilities of the motor to the required translation. A calculation can be found in the Design Report, which shows that this required resolution can be achieved, based on the specifications of the motor, the gear ratio, and the pitch angle of the lead screw.

## III. DESIGN & IMPLEMENTATION

### A. Concept

Based on a static version conceived by G. Millet [1], a device was designed to activate a braking mechanism that could fit inside a shoe. A full report on the design of the device can be found in the Appendix.

Two unique challenges exist in this design. The first being fitting a suitable source of motion into a small volume. The second being turning this motion into a precise, translational movement. To put the driving force into the shoe, a good solution is to use a small electric motor, powered externally by a battery. For robust, precise, low velocity rotation, a stepper motor is used. Specifically, a thin-profiled motor is implemented, called a "pancake stepper motor[1]," which is able to fit into the small volume, while providing enough torque to activate the brakes. To convert this rotational motion into

[1] http://www.moonsindustries.eu/

translational motion, a lead screw[2] is used. A lead screw is the ideal simple machine to do this efficiently because it is not back-drivable, meaning an axial load cannot transmit a torque back onto the motor. To transport the rotational motion from the motor to the brakes, with little energy losses, an effective method is to use a gear train. Intermediate gears are placed on either side of the motor and drive the outermost gears, which are fixed to the lead screws.

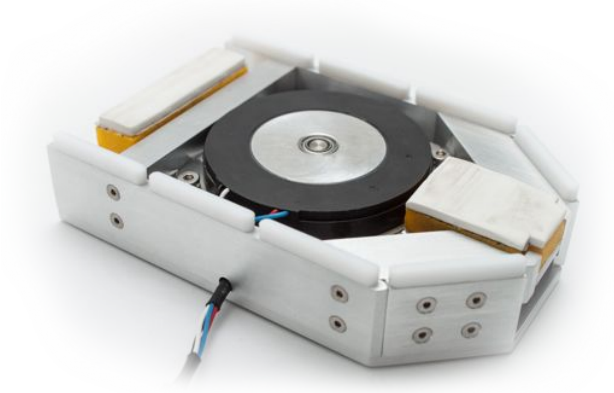

Fig. 1. The finished prototype

A plate, shaped to fit on the heel of a shoe, holds these components in the center of the device and small walls surround the driving mechanism, which support the low-friction material.

### *B. Detailed Design*

Given the unique set of constraints placed on the design of this mechanism, some of the details required to satisfy the requirements are especially noteworthy and are described below.

*1) Bearings & Gears:* To allow fluid rotation, while taking the full load of the user's weight directly onto the gears, two radial bearings are used for each gear. Embedding a flanged ball bearing into both sides of each gear, and running a hub through the center and into the base plate, the gears are fully supported. A spacer in between the two bearings and a spacer between the inner ring of the lower bearing and the base plate ensure that the axial load is transmitted directly through the bearings and into the plate, without affecting the rotation. Figure 2 shows a schematic of this. Any bending moment on the gear is also supported, as the two bearings are coupled about the gear, and the radial loads should be negligible, as the gear system is symmetrical. There is a total of five gears, with the central gear fastened to the motor shaft, and not requiring any bearings, two intermediate gears and two gears that support the brakes.

*2) PTFE Walking Surface:* PTFE is a soft material known for its non-stick properties, but is resistant to adhesives, so making the primary walking surface of a shoe with it is non-trivial. In order to create a smooth, secure slip surface around the perimeter of the mechanism, without gluing or screwing

[2]http://www.roton.com/

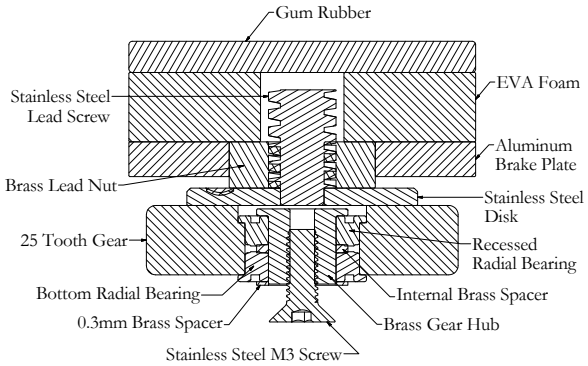


Fig. 2. Cutaway showing details of the bearings, gears and brake

it in, a set of (Teflon® brand[3]) PTFE tabs was manufactured that could be inserted into the walls of the device. The tabs, machined from a block of PTFE and snapped into slots along the edges of the walls, provide a thin, rigid walking surface with a low coefficient of friction. The aluminum walls which contain the PTFE tabs are fastened to the the frame of the device, and supported such that the axial load from a step is transmitted into the base plate.

Fig. 3. Teflon support detail

*3) Lead Screw & Nut:* A lead screw and nut combination is used to turn the gears' rotational motion into translational motion of the brake plate. To achieve this, the screw is turned down on one end and brazed into the center of a disc, which is then screwed onto the top of the braking gear. A lead nut is machined down so it can be embedded into the brake plate, which is then threaded onto the lead screw. The brake plate has a block of elastic EVA foam[4], and a strip of gum rubber[5] adhered to it, with a hole for the lead screw to recess into when it descends. For both front and rear brakes, an aluminum support restricts rotation so that when the lead screw rotates, the whole brake can only translate.

*4) Materials:* Strength is balanced with weight and machinability, when choosing proper materials, so aluminum makes up the majority of the components, with choice features being

[3]http://www2.dupont.com/Teflon
[4]http://www.zotefoams.com/
[5]http://www.staedtler.com/

Fig. 4. Lead screw detail

brass or stainless steel. Brass was used for spacers and hubs, where machinability was the main concern, and stainless only used for the lead screw, lead screw disk, and gears, where strength and ability to braze were necessary.

### C. Manufacturing

This device requires about 40 components to be machined and involves milling, turning, CNCing, drilling, tapping, brazing, and gluing. These duties were shared between the student and the technician, Donald Pavlasek, and completed over a one month period. Great care was taken to ensure proper tolerances were met in the machining of every part, as the alignment and rotation of the gear system, and the movement of the brakes, required it.

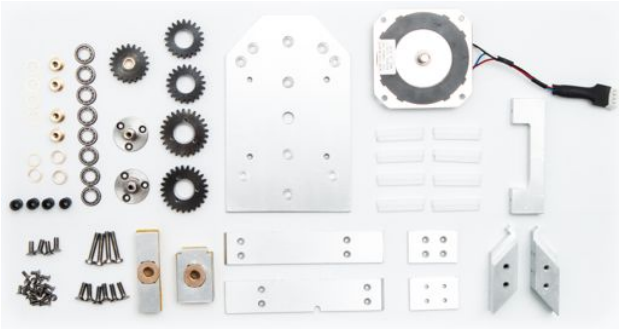

Fig. 5. All of the machined components

### D. Control

To control the height of the brake plates, via the steps of the stepper motor, a stepper motor controller[6] was wired to an Arduino microcontroller[7], and powered externally with 12V DC power. There are many options available to then control the motor, which depend on the fidelity required and the use case. For discrete, precise, and repeatable results, a digital input could be employed via serial or wireless connection, and using typed values or button inputs. For a simple proof of concept, however, an analog signal was used, by adding a potentiometer to the analog inputs of the microcontroller, and mapping the range of the dial to the range of motion of the brake.

*Open Loop Proportional Controller:* The control installed on the microprocessor is a simple open loop, proportional controller with a moving average filter on the analog input. The potentiometer was mapped to the total number of micro steps it took the motor to reach the full range of height, and then divided into to twenty intervals. The moving average filter filters the noisy analog signal, and the difference between the current input and the last input is taken as the proportional error. The motor is then commanded to move a number of steps equal to the normalized analog input times the total number of micro steps. Unfortunately there is no feedback in the loop, so we have to assume that the desired height is reached with every command, but this is a fair assumption given the accuracy of the stepper motor.

[6] https://www.sparkfun.com/products/10267
[7] http://arduino.cc/en/Main/arduinoBoardLeonardo

## IV. Conclusions & Future Work

Simple proof-of-concept tests have proven successful, meaning tangible changes in friction are apparent when sliding the mechanism across a PTFE surface while adjusting the height of the brakes with a potentiometer. Higher fidelity control and proper tests must still be done, however, and will be completed in summer 2014.

### A. Improvements

Open loop control is not reliable, as disturbances cause errors that cannot be adjusted for, so a closed loop control scheme is preferred. To allow for proper closed loop control, an encoder could be placed near the motor to send positional feedback, which would make up for an overloaded motor or skipped steps.

Another issue is that the motor is not powerful enough to extend the brakes under the load of the user, which is essentially lifting the user's weight, and so should only be used in that direction in between paces. A load cell embedded in a brake would signal when the force is low enough for the motor to be powered, saving the motor from stalling frequently and improving the accuracy of the controller.

### B. Controller Development

A higher fidelity controller is desired, which would involve closed loop control, digital inputs, and a wireless interface. Including the inputs of the sensors, to provide estimated pose, will simply close the control loop, but greatly improve accuracy. Implementing a wireless interface would mean adding a wireless shield to the microcontroller, to send inputs over wifi, and those digital inputs could be precisely mapped heights sent by the tester for very high resolution. Additionally, a smaller microcontroller could be used, with the hardware installed permanently and efficiently, to minimize the overall profile.

### C. Tests

To properly demonstrate the performance of the device, the first test to conduct is the tilt test. The mechanism is placed on a long, even surface of PTFE, with motion tracking markers mounted to it, and then the whole surface is slowly tilted and tracked using motion capture. The tangent of the angle at which it begins to slip is the coefficient of static friction, and its acceleration, measured with the motion capture, can give us the kinetic friction coefficient. This will be repeated until each level of friction that was initially required has a height value associated with it.

When the encoder and load cell are installed, additional tests must be carried out to measure the maximum load the motor can handle and evaluate the performance of the encoder. Once the sensors are calibrated and working with the control, higher fidelity tests begin with the device installed in a shoe. The device must be shown to handle the loads of a walking user, produce natural-feeling slip scenarios, and not impede natural walking.

### D. Natural Interactive Walking

One of the applications for a variable-friction shoe mechanisms is in the Natural Interactive Walking environment, of the CIM lab at McGill University [8]. This virtual environment (VE) immerses the user via simulated visual, auditory, and tactile senses. External projectors shine outdoor scenes on screens surrounding the user, and onto the floor surface. The floor is made of vibrotactile tiles, with sensors and actuators embedded in them, which sense foot steps and move to mimic the feeling of a real surface, such as cracking ice or snow. The addition of variable friction to this environment could greatly increase the fidelity of the simulated experience. Once the functional requirements of the device have been met with tests, it could be implemented into this virtual environment.

## ACKNOWLEDGMENTS

The author would like to thank Guillaume Millet for his contribution through past research results and input on design decisions. He would also like to thank Don Pavlasek, who offered his experience with design and spent many days manufacturing the components.

## REFERENCES

[1] G. Millet, M. Otis, and J. R. Cooperstock, "Variable-friction devices for friction-controlled walking." Unpublished.

[2] G. Millet, M. Otis, and J. R. Cooperstock, "Vibration-induced friction control for walkway locomotion interface," in *IEEE International Conference on Systems, Man, and Cybernetics*, p. 3961, 2013.

[3] V. Scott, L. Wagar, and S. Elliott, "Falls & related injuries among older canadians: fall-related hospitalizations & intervention initiatives," tech. rep., Public Health Agency of Canada, 2010.

[4] J. M. Hausdorff, D. A. Rios, and H. K. Edelberg, "Gait variability and fall risk in community-living older adults: A 1-year prospective study," *Archives of Physical Medicine and Rehabilitation*, vol. 82, no. 8, pp. 1050 – 1056, 2001.

[5] L.-W. Chu, I. Chi, and A. Chiu, "Incidence and predictors of falls in the chinese elderly," *Annals, Academy of Medicine, Singapore*, vol. 34, no. 1, pp. 60 – 72, 2005.

[6] H. Luukinen, K. Koski, L. Hiltunen, and S.-L. Kivela, "Incidence rate of falls in an aged population in northern finland," *Journal of Clinical Epidemiology*, vol. 47, no. 8, pp. 843 – 850, 1994.

[7] A. Roberts and J. Richardson, "Interface study of rubber-ice friction," *Wear*, vol. 67, no. 1, pp. 55 – 69, 1981.

[8] Y. Visell, A. Law, J. Ip, R. Rajalingham, S. Smith, and J. R. Cooperstock, "Interaction capture in immersive virtual environments via an intelligent floor surface," in *IEEE Virtual Reality (VR)*, p. 313, 2010.

# APPENDIX

## CAD RENDERS

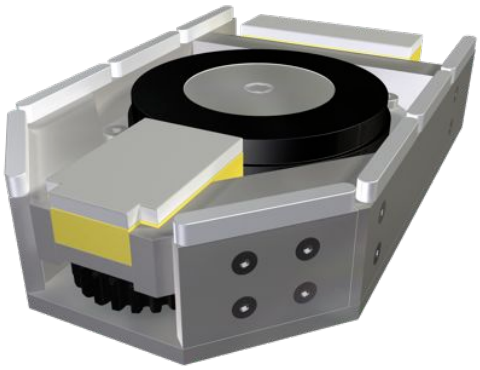

Fig. 6. Isometric overview

Fig. 7. Isometric bottom view

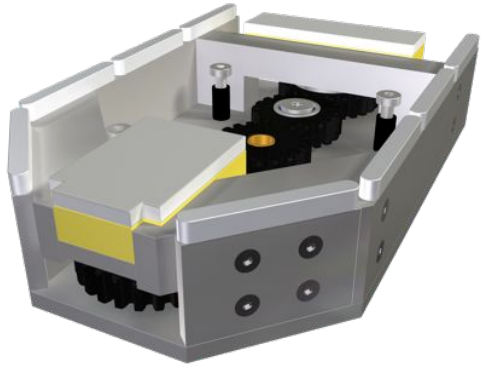

Fig. 8. Isometric overview without motor

Fig. 9. Side view

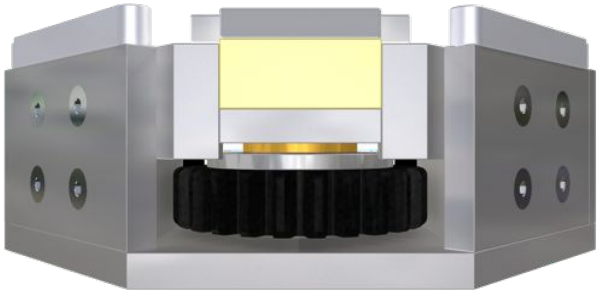

Fig. 10. Rear view

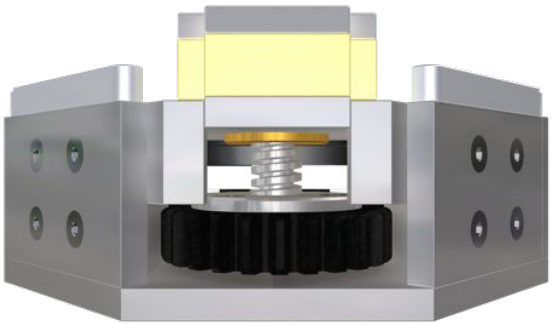

Fig. 11. Rear view with brake up

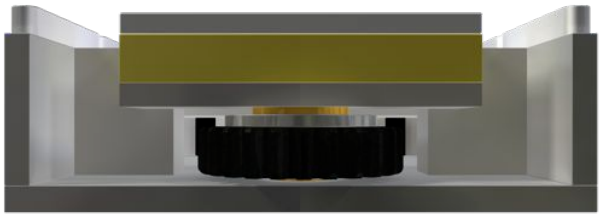

Fig. 12. Front view

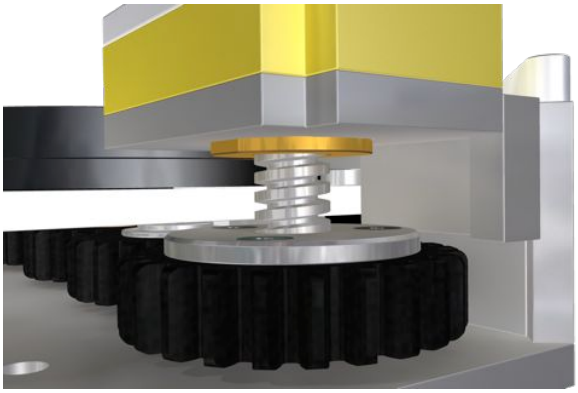

Fig. 15. Brake detail

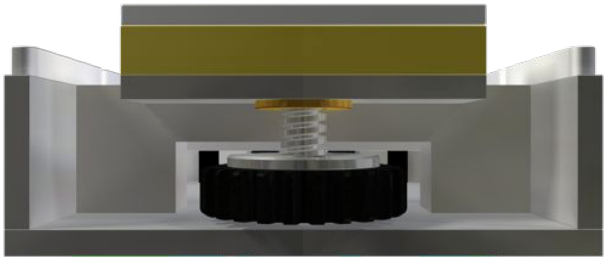

Fig. 13. Front view with brake up

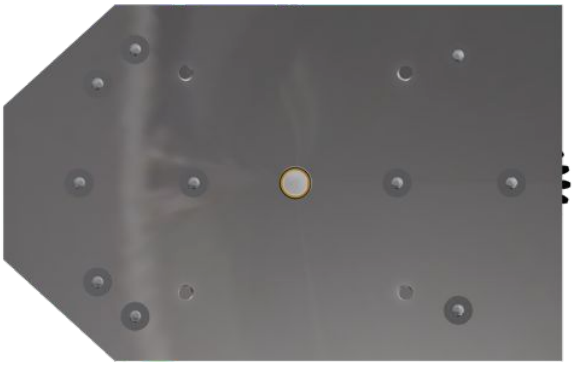

Fig. 16. Bottom view

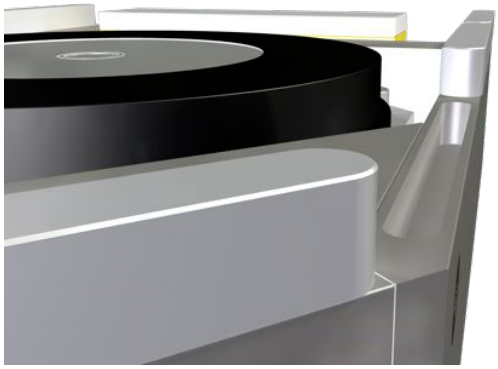

Fig. 14. Teflon detail

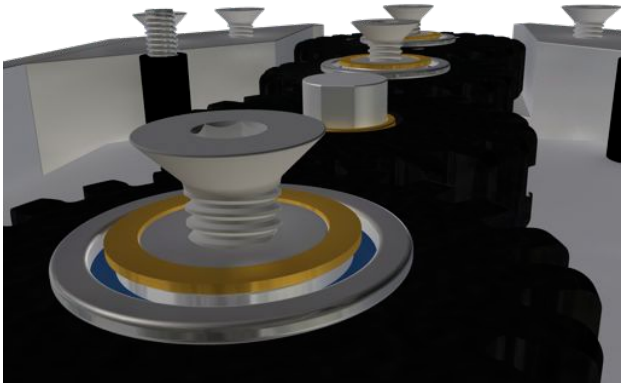

Fig. 17. Bearing detail

## PHOTOGRAPHS

Fig. 18. Finished prototype

Fig. 19. Overview from the bottom

Fig. 20. Base plate

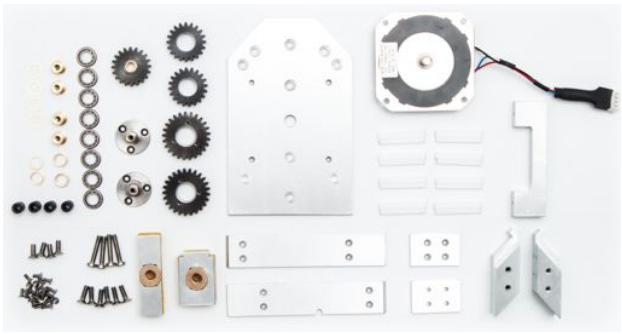

Fig. 21. All the components

Fig. 22. Bearings

Fig. 23. Front brake

Fig. 24. Rear brake

Fig. 25. Brake gear

Fig. 26. Front brake support

Fig. 27. Rear brake support

Fig. 28. Components of one gear

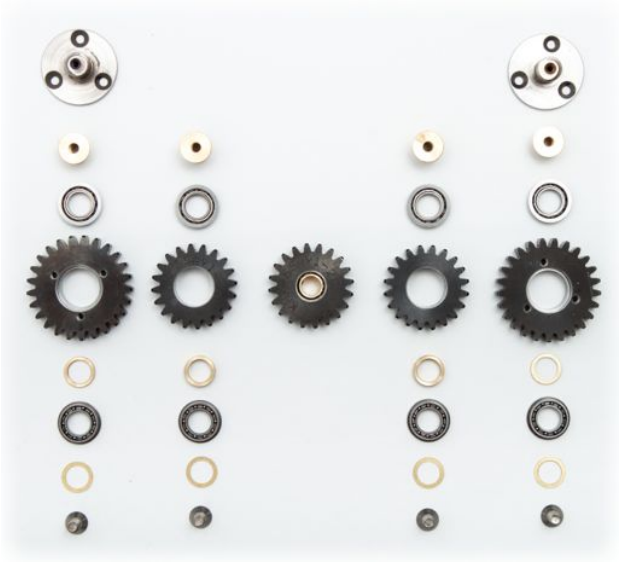

Fig. 29. Components of all the gears

Fig. 30. Three sizes of brass spacers

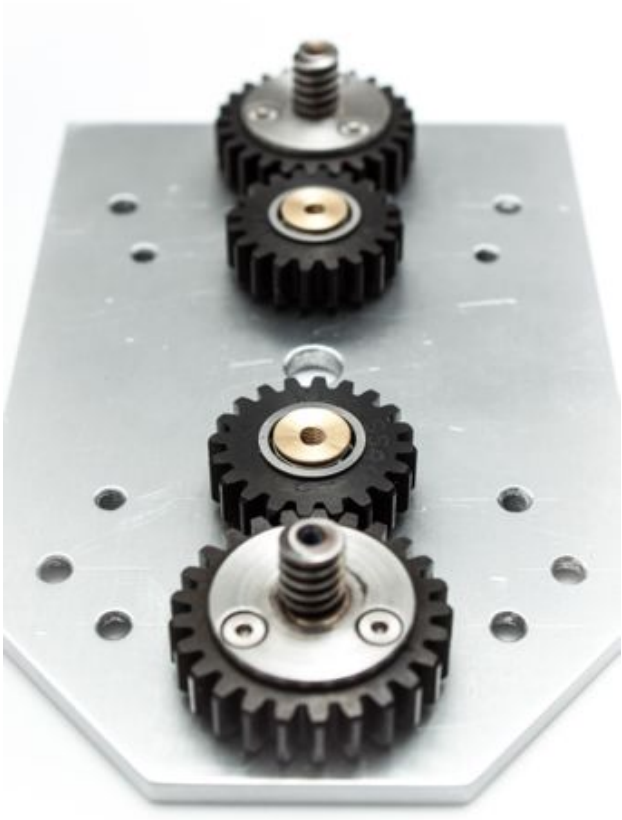

Fig. 31. The gears attached

Fig. 32. Gear hubs

Fig. 33. The intermediate gear

Fig. 34. The intermediate gear with bearings installed

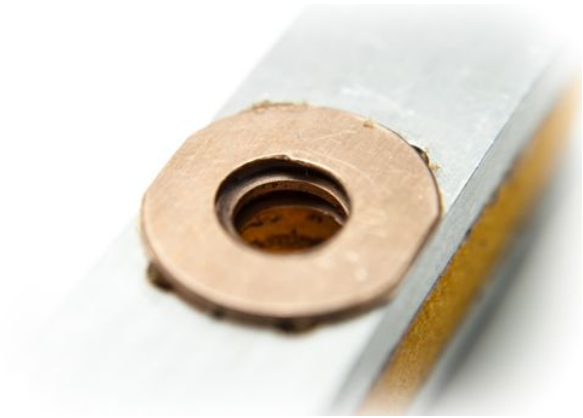

Fig. 35. Lead nut embedded in the brake plate

Fig. 36. Lead screw

Fig. 37. Lead screw installed on gear

Fig. 38. Motor gear

Fig. 41. Motor spacers

Fig. 39. Motor gear with tapped hole for set screw

Fig. 40. Stepper motor

Fig. 42. Teflon support

Fig. 43. Teflon support detail

Fig. 44. Short Teflon support

Fig. 45. Long Teflon support

Fig. 46. Teflon tabs

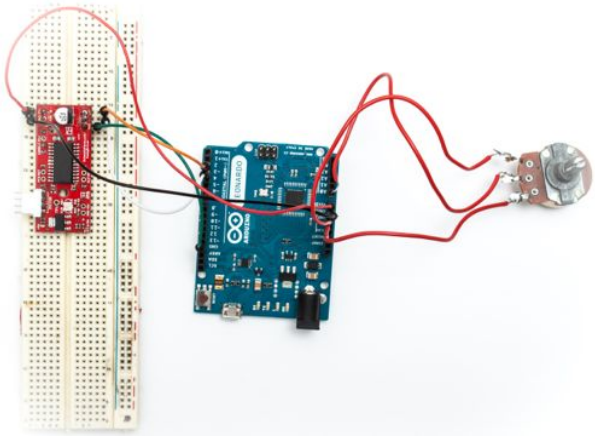

Fig. 47. The motor controller, microcontroller, and potentiometer

## CONTROL CODE

```
int dirPin = 2; // pin that controls direction
int stepPin = 3; //pin that controls stepping

int setPoint; // desired position
int currentHeight = 0; // estimated current height (last setPoint)
int error = 0; // initialize error
const int INTERVALS = 20; // number of intervals to split up full height into
int sensorVal = 0;

// MOVING AVERAGE VARIABLES
const int NUMBERSAMPLES = 3;
int samples[NUMBERSAMPLES] = {0};
int pointerInSamples = 0;

const int STEPS = 3000; // total number of microsteps from all
                                                    // the way down to all the way up - CALIBRATE -

void setup() { //declare Outputs
pinMode(dirPin, OUTPUT); //direction
pinMode(stepPin, OUTPUT);
}

// MOVING SAMPLE
void addSample(int newSample){
  samples[pointerInSamples] = newSample;
  if(pointerInSamples == (NUMBERSAMPLES - 1)){
  pointerInSamples = 0;
  }
   else pointerInSamples++;
}

// AVERAGE VALUES
int getAverage() {
 int sum = 0;
  for (int i =0 ; i<NUMBERSAMPLES; i++){
 sum = samples[i] + sum;
 }
 int avg = sum/NUMBERSAMPLES;
 return avg;
}

// CHANGE THE HEIGHT WITH OPEN LOOP CONTROL
void changeHeight(){
  if (error > 0){
     digitalWrite(dirPin, LOW);      // Set the direction
  }
  else {
    digitalWrite(dirPin, HIGH);      // Set the opposite direction
  }
  for (int i = 0; i < abs(STEPS*error)/INTERVALS; i++)
  {
    digitalWrite(stepPin, LOW);  // This LOW to HIGH change is what creates the
    digitalWrite(stepPin, HIGH); // "Rising Edge" so the easydriver knows to when to step.
    delayMicroseconds(470);      // Delay time. ~270 is fastest before stalling with 12V (shor
  }
}
```

```
// MAIN LOOP
void loop() {

  addSample(analogRead(A0));           // read the value from the sensor and add it to the movi
  setPoint = map(getAverage(), 0, 1023, 0, INTERVALS); // map the average value from the poten
  error = setPoint - currentHeight;     // calculate the proportional error
  changeHeight();          // change the height based on the total number of steps and the numb

  // print the results to the serial monitor:
 Serial.println(setPoint);    // prints the desired interval

  currentHeight += error; //add the error to the current height, which assumes you reached the
  delay(100); // in milliseconds

}
```

# SUPPORTING DOCUMENTS

Parts & Materials Order

| Status | Supplier | Part # | Material | Description | Size | Package | Qty | Need Qty | Cost | Part | Part |
|---|---|---|---|---|---|---|---|---|---|---|---|
| Order Online | McMaster | 93395A137 | Stainless Steel | M2 Flat Head Socket Screws | M2 5L | 25 | 2 | 22 | $14.40 | Teflon Supports | Drive Shaft Flange |
| Order Online | McMaster | 93395A204 | Stainless Steel | M3 10L Flat Head Socket Screws | M3 10L | 100 | 1 | 6 | $10.53 | Brake Guide Front | Break Guide Rear (2) |
| Order Online | McMaster | 93395A201 | Stainless Steel | M3 8L Flat Head Socket Screws | M3 8L | 100 | 1 | 4 | $11.26 | Gear Hubs | |
| Order Online | McMaster | 92605A502 | Stainless Steel | M2 Set Screws | M2 4L | 5 | 1 | 2 | $9.59 | Motor Gear | |
| Order Online | McMaster | 92855A316 | Stainless Steel | M3 Cap Hear Socket Screws | M3 16mm | 25 | 1 | 4 | $3.20 | Motor | |
| Order Online | McMaster | 93657A714 | Nylon | Motor Bolt Spacer | M3 | 1 | 6 | 4 | $6.66 | Motor | |
| Order Online | QTC Gears | SSAY1-20 | Steel | 20 Tooth Hubless, Thin Face Spur Gear | 20mm | 1 | 4 | 3 | $29.24 | Intermediate Gears | |
| Order Online | QTC Gears | SSAY1-25 | Steel | 25 Tooth Hubless, Thin Face Spur Gear | 25mm | 1 | 2 | 2 | $16.06 | Brake Gears | |
| Quoted | Moon's Industries | 23HM6401 | - | Pancake Stepper Motor (6401 is 11mm) | 11mm | 1 | 1 | 1 | $36.00 | Motor | |
| Order Online | Roton | 59792 | Stainless Steel | 1/4"-16 Lead Screw | 1/4"-16 | 1 | 1 | 2 | $21.74 | Lead Screw | |
| Order Online | Roton | 89712 | Bronze | 1/4"-16 Lead Nut | 1/4"-16 | 1 | 2 | 2 | $51.88 | Lead Nut | |
| Order Online | BearingsDirect.com | MF106 | - | 6x10x2.5 Open Mini Bearing | | 1 | 10 | 8 | $32.50 | Bearings | |
| Order Online | Sparkfun | ROB-10267 | - | EasyDriver Stepper Motor Driver | | 1 | 1 | 1 | $14.95 | Motor Controller | |
| | | | | | | | | **Total** | $258.01 | (before tax/shipping) Prices in USD | |

Fig. 48. Orders spreadsheet

Bill Of Materials

| Part Name | Material | Dimensions | Supplier | Part # | Qty | Drawing | Drawn | Machining Status |
|---|---|---|---|---|---|---|---|---|
| PLATE-STEEL-HOLDER | Aluminum 6061 | 1/8"t 70x110mm | Stock | Steel plate MEDN | 1 | Y | Y | Complete |
| GEAR-QTC-SSAY1-20 | Stainless Steel | 20mm | QTC Gears | SSAY1-20 | 3 | Y | Y | Complete |
| GEAR-QTC-SSAY1_25 | Stainless Steel | 25mm | QTC Gears | SSAY1-25 | 2 | Y | Y | Complete |
| STEPPER_MOTOR-MOONS-23HY9401 | - | - | Moons Industries | 23HM6401 | 1 | N | - | Arrived |
| BRAKE-FRONT-EVA | EVA Zote Foam | 45x12 | Stock | - | 1 | N | - | Complete |
| BRAKE-FRONT-RUBBER | Rubber | 45x12 | Stock | - | 1 | N | - | Complete |
| BRAKE-FRONT-STEEL | Aluminum 6061 | 45x12 | Stock | - | 1 | Y | Y | Complete |
| BRAKE-REAR-STEEL | Aluminum 6061 | 30x20 | Stock | - | 1 | Y | Y | Complete |
| BRAKE-REAR-EVA | EVA Zote Foam | 30x20 | Stock | - | 1 | N | - | Complete |
| BRAKE-REAR-RUBBER | Rubber | 30x20 | Stock | - | 1 | N | - | Complete |
| LEAD_SCREW-NORDEX-MAS_A2_8 | Stainless Steel, 440C | 1/4"-16 x 1ft | Roton | 89712 | 2 | Y | Y | Complete |
| LEAD_NUT-ROTON-89712 | Bronze | 1/4"-16 x 1/2" | Roton | 89712 | 2 | Y | Y | Complete |
| SPACER-MCMASTER- 93657A714 | Nylon | M3 | McMaster | 93657A714 | 4 | N | - | Arrived |
| BRAKE-GUIDE (FRONT) | Aluminum 6061 | 18x9x48.5 | Stock | - | 1 | Y | Y | Complete |
| GEAR-HUB | Brass | | Stock | - | 2 | Y | Y | Complete |
| GEAR-HUB-LONG | Brass | | Stock | - | 2 | Y | Y | Complete |
| GEAR-SPACER | Brass | | Stock | - | 2 | Y | Y | Complete |
| GEAR-SPACER-THICK | Brass | | Stock | - | 2 | Y | Y | Complete |
| BEARING-SPACER | Brass | | Stock | - | 5 | Y | Y | Complete |
| BEARING-RADIAL-NSK-MR106 | Stainless Steel | | BearingsDirect | MF106 | 8 | N | - | Arrived |
| TEFLON-SUPPORT_ANGLE | Aluminum 6061 | | Stock | - | 2 | Y | Y | Complete |
| TEFLON-SUPPORT_SIDE | Aluminum 6061 | | Stock | - | 1 | Y | Y | Complete |
| TEFLON-SUPPORT_SIDE1 (MIRROR) | Aluminum 6061 | | Stock | - | 1 | Y | N | Complete |
| BRAKE-GUIDE-REAR | Aluminum 6061 | | Stock | - | 1 | Y | Y | Complete |
| BRAKE-GUIDE-REAR1 (MIRROR) | Aluminum 6061 | | Stock | - | 1 | Y | N | Complete |
| TEFLON | Teflon | 1/8"t | Stock | - | 2 | Y | N | Complete |
| TEFLON-BRAKE_GUIDE | ? | 1/8"t | ? | - | 2 | Y | N | Not Needed |
| BOLT-M2-5-FLATHEAD-SOCKET-MCMASTER-91294A003 | Stainless Steel | M2 5L Flat Socket | McMaster | 93395A137 | 22 | N | - | Arrived |
| BOLT-M3-8-FLAT_HEAD-SOCKET-MCMASTER-93395A201 | Stainless Steel | M3 10L Flat Socket | McMaster | 93395A201 | 6 | N | - | Arrived |
| BOLT-M3-16-MCMASTER-92855A316 | Stainless Steel | M3 16L Socket | McMaster | 92855A316 | 4 | N | - | Arrived |
| BOLT-M3-8-FLAT_HEAD-SOCKET-MCMASTER-95A201 | Stainless Steel | M3 8L Flat Socket | McMaster | 93395A201 | 4 | N | - | Arrived |
| SET_SCREW-M2-4-MCMASTER-92605A502 | Stainless Steel | M2 4L Set Screw | McMaster | 92605A502 | 2 | N | - | Arrived |
| DRIVE_SHAFT-FLANGE | Stainless Steel | | Stock | - | 2 | Y | Y | Complete |

Fig. 49. Bill of materials

# DESIGN REPORT

*Interdisciplinary Design — Design Report*

# Development of a Variable-Friction Shoe Surface Mechanism

Michael Elliot King – 260345001

MECH 498 – Professor Rosaire Mongrain

*Client & Supervisor:* Professor Jeremy Cooperstock

Department of Mechanical Engineering

**McGill University**

December 6, 2013

**Abstract**

In order to treat and prevent accidents caused by balance-failure and friction-induced falls, a proper simulation environment is needed so users can be exposed to controlled slip conditions and trained to improve balance. This report covers the design of a mechanism that fits in the sole of a shoe and can dynamically actuate a brake that varies the coefficient of friction between the shoe and the walking surface. As it is vital to replicate a realistic sense of walking and slipping, the mechanism must be non-obtrusive and high-fidelity, and able to simulate a continuous range of surfaces, such as ice, wet grass, sand, or snow.

# Contents

# List of Figures

# 1

# Introduction

The idea of developing variable-friction devices for friction-controlled walking has been researched and prototyped by the *Shared Reality Lab of the McGill Centre for Intelligent Machines* under the supervision of Professor Jeremy Cooperstock [1]. Their research has been into the development of a variety of actively controlled floor surfaces, including vibration-controlled friction, ball transfer units, and braking pins, as well as a vibrotactile shoe mechanism. This new design is of a shoe mechanism that uses a static slip surface and an active braking surface to vary the coefficient of friction on a specific passive floor surface.

## Background

In the following explanation of the motivations behind the proposed work, the draft manuscript from a previous study is paraphrased, which includes some references to statistics concerning balance failures [1]. In the age group of those 65 years and older, falls are the cause of 88% of injuries [2], and can lead to their loss of independence and even death. It has been shown in Canada [2], the United States [3], China [4], and Finland [5], that one in three of those this age will fall once a year. Dealing with these injuries involves preventative measures, such as studying the way people walk and react to walking surfaces, as well as rehabilitation, like balance and mobility training. For rehabilitation training, simulated environments must be created to properly imitate the slip environments that cause people to fall. This requires the

control of such an environment, by creating a surface with a dynamic coefficient of friction, similar to a natural environment with real obstacles.

Designing a variable-friction walking surface has the potential to be useful in clinical or rehabilitation applications to simulate low-friction induced accidents. Research has been completed already to create a floor surface with very low coefficients of static friction, but has proven to be limited in supported footwear and in simulating natural walking patterns. The technology and expense behind creating a useful walking surface is also a limiting factor. By developing a shoe with the capabilities of varying the friction at the contact surface, more possibilities exist for floor types, and simulating natural walking becomes easier. The main challenge remains to be implementing the proper technology into the sole of a shoe, hence the inspiration for such a project.

# Problem Definition

A lot of research has already been done to provide the resources for the design of a variable-friction shoe surface. Professor Cooperstock's lab has provided the foundation for this project with background information and even high-level concepts, off which a design can be based. They studied the mechanics behind natural human walking, regarding the forces of friction that cause slipping and how they can be controlled. The materials and methods that could be used for friction control were studied and design criteria defined.

The general concept for the design, created by Millet [1] over the past summer, involves varying the amount of contact between the floor and two shoe-surfaces of different coefficients of friction. One has a very low CoF, similar to that of ice, and the other a very high CoF. By varying the amount the high-friction surface protrudes from the low-friction surface, the weight distribution between the two surfaces changes, and this is proportional to the total effective friction force. When the translation of the high-friction surface is actively controlled, it acts like a brake, and the effective CoF, $\mu_{effective}$, can be varied dynamically while someone is walking. By introducing a sudden change in friction during a natural stride, a simulated slip environment is created. A fully static prototype of a shoe mechanism such as this was created and tested by Millet and is shown in Figure 1.1.

Figure 1.1: Early prototype of a static variable-friction shoe device by G. Millet [1]

The main challenge is to come up with a suitable mechanism that can carry out the necessary actions to successfully vary the friction, while satisfying the design requirements and fitting within the given constraints.

## Design Requirements

To facilitate proper design, explicitly laying of the requirements of the design is a useful practice. As the design has evolved, the requirements have changed slightly, to reflect the focus of the actual prototype.

The device must:

- Contain one more mechanisms
- Be actively controlled
- Embed all mechanisms into the sole of a shoe
- Bear the load of a person on one surface
- Effectively change the friction coefficient of the shoe-ground interface

# 2

# Conceptual Design

Working with Guillaume Millet, the Postdoctoral researcher who did the preliminary research on a mechanism that would fit into a shoe sole and consist of a passive low-friction surface and an active high-friction surface, we created some design criteria, generated possible concepts, analyzed the concepts and chose the best one.

## Evaluation Criteria

In order to optimize the design, a set of criteria was created with which we could weigh and analyze the different concepts. This typically means maximizing efficiency, or increasing output and decreasing input. In this case, input is cost, weight, and complexity, and output is load and robustness. Additionally, and most importantly, the mechanism must be small enough to fit into the sole of a shoe and permit natural walking.

### Cost

Something to always consider, while not a priority in this, is the cost and financial feasibility of the design. This design was budgeted at about $350, and although not due to limited funds, it would not be practical to create a design much more expensive than this. When researching materials, components, and manufacturing methods, this must be considered.

### Weight

As part of the design requirement that the mechanism permit natural walking, weight must be reduced as much as possible, as to not create an unnatural load on the user's feet. The target weight is set at 1kg per mechanism, as this is near to what a work boot weighs, which is the heaviest type of footwear the average person wears.

### Complexity

Fewer moving parts and less complexity is almost always a goal in design, and in a design that must function and fit into the sole of a shoe, this is paramount. Moving parts mean space to move more degrees of freedom, which is difficult to implement in such a confined space. Additionally, the mechanism is required to hold the weight of a person, and a less constrained design means more places for failure.

### Robustness

Stemming from the design requirement that the device must have a standing load of one person – about 700N - and handle the stresses of a person's stride, the design must be very robust. It needs to be able to use parts and materials that are strong enough to handle these loads, while still meeting the other requirements.

### Size

The most important requirement is that the device is small enough to fit into the sole of a shoe. If the design cannot be made very small, than it is of no use, so size is the number one concern.

## Concept Generation

Some concepts were suggested to me by Millet (Appendix D.1), and sketches were sent along with the ideas to begin the concept generation. The main principle of the concepts to be

generated is the method of turning rotational motion into vertical translational motion. A linear actuator is designed to do exactly this, but given the size requirements and custom geometry, this must be specially designed.

**Wedges & Cable** One idea is to utilize the mechanical advantage of two wedges, placed on top of each other, so that when they are forced inwards, they slide up each other's slope and cause an overall translation perpendicular to the input force. The input force would be driven my a motor, and converted to linear motion via a cable and system of pulleys.

**Cam** A similar idea to the wedge is to use a cam. The shape of a wedge essentially combines a cylinder with a ramp, so that rotational motion can easily be converted to translational motion, like in a car engine.

**Worm Gear with Rack & Pinion** Onto the idea of using gears, one method would be to drive a gear that spins a worm to transfer the rotational motion 90°, and then a rack and pinion to create the linear motion. A preliminary sketch of this can be found in Appendix D.2.

**Lead Screw** The other gear device involves one gear driving another gear, which is fixed to a lead screw. The lead screw is threaded into a lead nut, which converts the rotational motion to linear motion when its rotation is constrained (Appendix D.3).

# Concept Evaluation

**Wedges & Cable** This concept excelled in the weight and cost criteria, as small cables and pulleys are much lighter and cheaper than cams and gears, but it lacked in robustness, simplicity, and size. Immediately, this seemed extremely difficult to implement on such a small scale, as cables need to be strong and tight, and their ductility becomes a large source of error when dealing with movements that are fractions of a millimeter. Additionally, the complexity of running cables through pulleys, securing them and calibrating the system is a large drawback.

**Cam** The cam idea is simple and elegant, assuming friction can be dealt with properly using a cam follower. The weight and cost are both also favorable. The weakness of this setup is the robustness. Having a cam and cam follower bear all the load of a person is not possible with the given geometry.

**Worm Gear with Rack & Pinion** While this seems like a good idea in theory, worm gears are only intended to be driven by the worm, not the gear. In order to achieve the proper motion, the geometry of the worm and gear setup would have to change dramatically, and this would reverse the gear ratio and render the mechanism useless.

**Lead Screw** Lead screws can be very robust, and are designed to handle a large static load because friction does not allow the force to be transferred to the gears. The gear train and motor laid sideways are very compact, and for the loads the mechanisms will have, the lead screw does not have to be large. This design is rather heavy, however, as it involves a lot of metal parts, which also makes it expensive. As far as complexity, it does have a lot of moving parts, but the implementation is straightforward, so it is neither a drawback nor an advantage.

# Final Concept

The decision was made to go with the lead screw mechanism, for its robustness, and its ability to be implemented into such a small space. The complexity and weight are not favorable, but are of less importance, so they are a necessary deficiency of the design.

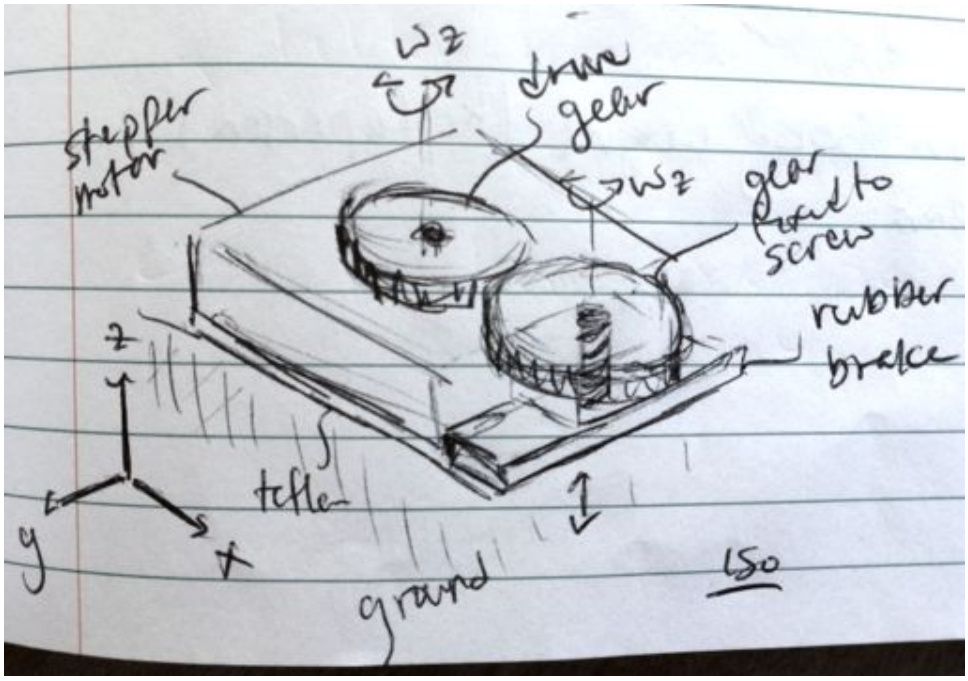


Figure 2.1: Lead screw concept

The idea of the lead screw design is to have a flat stepper motor fixed to a gear that drives a gear train as seen in Figure 2.1. The last gear in the train is fixed to a lead screw that is threaded into a plate, which acts as the lead nut. The plate is the base for a "brake," which consists of a rubber sheet and a block of EVA foam. The whole "brake" is what translates vertically, as its rotation is constrained while being driven by the lead screw, just like a tube of deodorant (Figure 2.2). Surrounding this mechanism along the perimeter are supports that hold a thin strip of Teflon, or PTFE, that acts as the main contact with the ground. Both the mechanism and perimeter supports are attached to a base plate, which is shaped like the heel of a shoe, and provides support for the entire device. This plate is what is embedded into the sole of a shoe or boot, in place of the existing heel. Once this concept is prototyped, it should be simple enough to duplicate and add to the front of the shoe for full friction control.

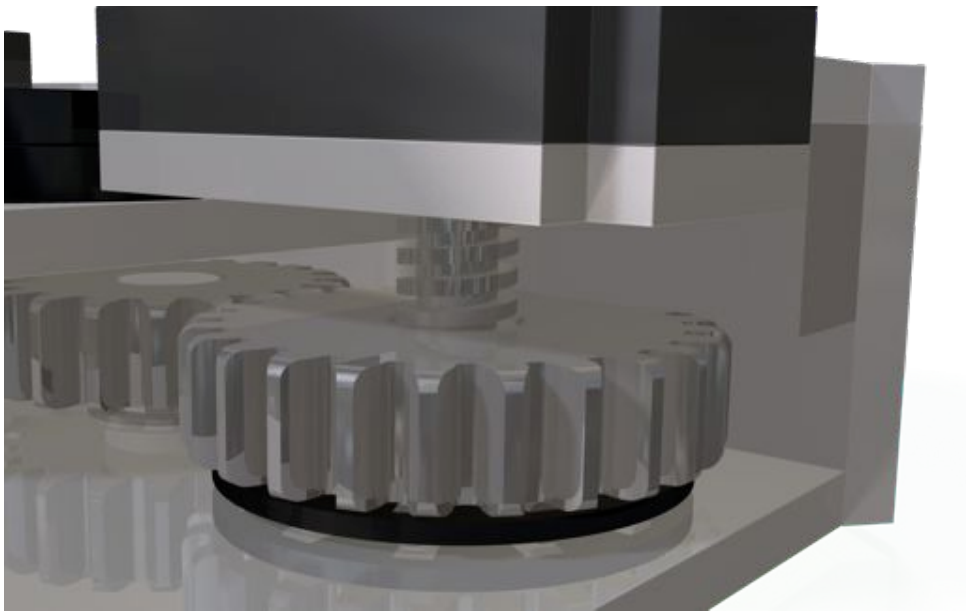

Figure 2.2: Close up of the brake design

# 3

# Embodiment Design

After studying the work by Guillaume Millet, Martin Otis and Jeremy R. Cooperstock, and reviewing their equations, I had to do some calculations of my own. Once calculations were done, the proper sizes and dimensions were known, and the design began to fall into place. I based my initial vision of the device on what Millet had sketched and prototyped, and began designing the lead screw mechanism into that. As the design progressed, the most challenging part was satisfying the load and size requirements of the design. As more details were added for the sake of robustness, the size constraint became more important. In the end there were many iterations of the design, as necessary parts were added and the rest of the design would be altered to reflect those changes.

## Guidelines & Previous Research

The first concept to understand when starting this design, is what "variable friction" actually means. Variable friction means simulating many different levels of static friction on a spectrum that ranges from normal contact friction between a rubber sole and the ground (about $\mu = 0.3$) to slipping on something as slippery as ice (about $\mu = 0.06$) [6].

Within this range, it is important to define the necessary step size needed to achieve a smooth, varying friction, based on the needs of the simulation. We have chosen to use ten different variations of friction in the range of $\mu = 0.06$ and 0.3, with finer resolution as

friction approaches the slip condition (Table 3.1).

| | $\mu$ |
|---|---|
| 1 | 0.06 |
| 2 | 0.07 |
| 3 | 0.08 |
| 4 | 0.09 |
| 5 | 0.10 |
| 6 | 0.12 |
| 7 | 0.14 |
| 8 | 0.16 |
| 9 | 0.20 |
| 10 | 0.30 |

Table 3.1: Desired coefficients of friction (CoF)

**How to achieve these coefficients** The shoe sole is designed to incorporate a thin support with a slip surface that acts as the main contact surface, and an active brake mechanism as the secondary contact surface. Based off of the previous research, the ideal slip surface is Teflon, or PTFE, as its self contact friction, $\mu_S$, is about 0.05 [1]. The high friction surface should be rubber, in an attempt to reach $\mu = 0.5$, as this is the CoF of rubber on dry asphalt – a typical surface for a shoe. The active brake mechanism, with the rubber surface, is extended beyond the surface of the Teflon, so that both the Teflon and rubber make contact with the ground. Underneath the layer of rubber, the brake also has an elastic material. This elastic material allows the brake to deform when it makes contact with the ground, and it deforms until it is flush with the Teflon surface. As force is proportional to deformation, as shown in the next section, the more the brake deforms, the more force is exerted on it. This force is what determines the amount of friction force that is delivered by the shoe, and in turn controls the effective coefficient of friction. To determine exactly how to dynamically accomplish this with a mechanism, some calculations must be made.

# Calculations

To begin, we look at the underlying mechanics of what is going on at the brake, in general terms. The force of friction acting on one rubber brake is a product of the CoF of the rubber and the normal force from the human that is being transmitted to the brake as in Equation 3.1. It is this friction force that is ultimately being controlled.

$$F_{friction}^{brake} = \mu_{rubber} F_{human}^{brake} \tag{3.1}$$

Additionally, the force from the human causes a strain proportional to the Elastic Modulus of the brake material, causing the brake to deform quite a bit.

$$F_{human}^{brake} = \frac{E_{brake} S_{brake} \Delta L}{L} \tag{3.2}$$

When the deformation, $\Delta L$, is limited to the length of protrusion of the active brake mechanism, only the $F_{human}^{brake}$ that satisfies this equation will be transmitted through the brake. The rest of the force of the human will be supported by the slip material around the edges, and it is this relationship between the force on the brake and the slip surface that varies the friction. This is shown in Equation 3.3 given by Millet, Otis and Cooperstock [1].

$$F_{human} = F_{lowfriction} + F_{highfriction} \tag{3.3}$$

Equation 3.2 can be rewritten more generally as

$$F_{highfriction} = E_{elastic} S_{elastic} \varepsilon_{elastic} \tag{3.4}$$

and combined with Equations 3.3 and 3.1 to give the relationship between the coefficients of friction, and how the effective CoF is achieved (Equation 3.5).

$$\mu_{effective} = \mu_{lowfriction} + (\mu_{highfriction} - \mu_{lowfriction}) \frac{E_{elastic} S_{elastic} \varepsilon_{elastic}}{F_{human}} \tag{3.5}$$

where $F_{human}$ is the vertical force applied on the shoe, $F_{lowfriction}$ is the normal force on the low friction surface, $F_{highfriction}$ is the normal force on the high friction surface, $E_{elastic}$

is the Young's Modulus of the elastic element, $\varepsilon_{elastic}$ is the controlled deformation of the elastic material, $S_{elastic}$ is the surface area of the high friction surface, and $\mu_{lowfriction}$ and $\mu_{highfriction}$ are the respective coefficients of friction.

Using Equation (3.5) and assuming $E_{elastic}$, $S_{elastic}$ and $F_{human}$ to be constant, we can solve for $\varepsilon_{elastic}$ or $\Delta L$ for each desired $\mu_{effective}$. This will give us the required deformation, and therefore translation, needed to vary the friction by the desired amount.

The problem with this, however, is that these values are not constant. Both $S_{elastic}$ and $F_{human}$ vary with stride, and $E_{elastic}$ for the EVA foam elastic material can only be considered linear in the first 40% of deformation, as shown in Figure 3.1.

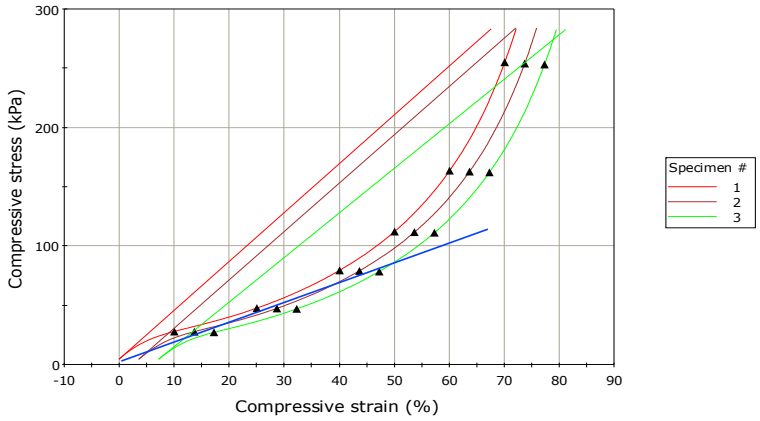


Figure 3.1: Compressive stress-strain curve of EVA foam (ZoteFoams)

To get around these issues and get an estimate, we consider only the linear region of the elastic material, as the small deformations ($\varepsilon_{elastic} < 40\%$) are what result in the lowest friction coefficients, and this is where the resolution is the smallest. At full brake extension, the elastic material can deform up to 80% (See Appendix A.10 for a visual of total brake extension) and at this strain, the Elastic Modulus becomes very high. The resolution for controlling the strain becomes large here, but precision is not needed.

Regarding the change in force and surface area over a stride, we can choose reasonable values for the calculations, but for proper testing, a force-torque sensor will be placed into the brake pad. The sensor will be able to sense when there is a load on that particular brake, which will give a nominal surface area (Equation 3.6)and a force reading. These readings will not necessarily be used in real time, but will at the very least make it possible to calibrate the device.

Total effective surface area given by:

$$S_{elastic,\ effective} = \sum_{i=1}^{n} S_{elastic,\ i} \tag{3.6}$$

where $n$ is the number of elastic elements and $S_{elastic} > 0$ if $F_{human} > 0$, as sensed by the F-T sensor.

To calculate the necessary resolution of the brake, we will consider the minimum load spread over the most area, for the least strain and therefore smallest resolution. The Elastic Modulus to be used will be 80kPa, as reported by G. Millet [1], and the $S_{elastic}$ and $F_{human}$ will be chosen to be the the surface area of two braking surfaces as shown in Equation 3.6 – totaling $0.00115m^2$ – and a $F_{human}$ of 350N – an average weight of a human on one shoe. Of course the actual value of $E_{elastic}$ will have to be tested for and the device calibrated, and proper force readings will be taken from the F-T sensors.

$$\varepsilon_{elastic} = \frac{(\mu_{effective} - \mu_{lowfriction})}{(\mu_{highfriction} - \mu_{lowfriction})} \frac{F_{human}}{S_{elastic} E_{elastic}} \tag{3.7}$$

Let's use:

$\mu_{low\ friction} = 0.05$

$\mu_{high\ friction} = 0.30$

$E_{elastic} = 0.080$ MPa [1]

$F_{human} = 350$ N

$S_{elastic} = 0.00115m^2$ $[20mm \times 30mm + 55mm \times 10mm]$

and $\mu_{effective} = [0.06, 0.07, 0.08, 0.09, 0.10, 0.12, 0.14, 0.16, 0.20, 0.30]$ 3.1

Putting this into MATLAB we get:

```
>> strain_resolution

strain =

    0.1458    0.2917    0.4375    0.5833    0.7292    1.0208    1.3125
1.6042    2.1875    3.6458
```

The results show that over 100% strain would be needed to achieve a $\mu_{effective}$ of 0.12,

which of course is impossible. This is due to the nonlinear elastic property of the material being modeled as linear. At this $\mu_{effective\ desired}$ and higher, the strain will certainly be nonlinear, and need to calibrated manually through testing. The important results from this are the strains closer to the slip condition.

The resolution needed is the difference between these smallest strain values:

$$\Delta\varepsilon_{elastic\ min} = |\varepsilon_{elastic}^{\mu=.06} - \varepsilon_{elastic}^{\mu=.07}| \tag{3.8}$$

where the necessary travel of the brake is $\Delta L$ given by:

$$\Delta L = \varepsilon_{elastic\ min} L \tag{3.9}$$

For $L = 6mm$ as defined by the thickness of the EVA foam, the minimum resolution $\Delta L$ is 0.8748mm.

This seems like a very small increment, but what is important is that the gear ratio, lead screw and stepper motor can make this small of a change. To begin, we start with the minimum rotation of the stepper motor, as this is the limiting factor. Equation 3.10 shows the minimum step size of the motor, as given by the manufacturer, to be 1.8°.

$$\theta_D = 1.8^\circ = \frac{1.8^\circ}{360^\circ} 2\pi = 0.0314\ rad \tag{3.10}$$

where $\theta_D$ is the step size of the stepper motor, or the minimum rotation of the driving gear. The rotation of the active gear is then just a function of the gear ratio:

$$\theta_{active} = \theta_D \frac{R_D}{R_{active}} \tag{3.11}$$

where we neglect the intermediate gear, since the ratio between the driving gear and the intermediate gear is 1:1.

Without choosing the lead screw first, we can calculate the pitch angle that would be needed to attain the desired resolution in one step of the motor.

$$\phi_{pitch} = \tan^{-1}(\frac{min\ resolution}{arc\ length\ of\ screw}) = \tan^{-1}(\frac{min\ resolution}{\theta_F R_{lead\ screw}}) \tag{3.12}$$

With a min resolution of 0.8748mm and $R_{lead\ screw} = 2.41mm$, the $\phi_{pitch}$ is 86.06°. This

maximum angle is much higher than the standard angle of a lead screw ($3° - 6°$), which means much more precision can be achieved by using a smaller pitch angle and having the motor spin many more times than the minimum step size. A few revolutions of the motor per minimum resolution means more fine tuned control at little cost.

By choosing a lead screw with the smallest lead makes the resolution smaller, and the friction lower. Using a 1mm lead and having a $R_{lead\ screw}$ of 2.41mm, the $\phi_{pitch}$ is 3.79°.

Based on the choice of lead screw, the number of revolutions of the motor per resolution step can be calculated. The angle of the lead screw is $\phi_{lead} = tan^{-1}(\frac{lead}{\pi D})$ and for the desired resolution, the angle of rotation of the lead screw and gear is $\theta_{active} = \frac{lead_{desired}}{tan\phi_{lead} R_{lead\ screw}}$. Using the gear ratio, as in Equation 3.11, it is clear that the driving gear and stepper motor must then turn $\theta_D = \theta_{active} \frac{R_{active}}{R_D} = 5.496\ rad$ or 314.9° to deliver the translational motion of one resolution to the braking surface. This means that the motor turns nearly one full revolution to deliver one change in resolution to the brake, which means excellent precision can be attained.

# Design Changes

The current design went through many iterations to get it right. Of course the original design will not work perfectly, so after reviewing the concept with Guillaume Millet and Professor Cooperstock many times, the design evolved and improved.

**First Iteration** The first design consisted of only three gears, one driving and two active, with a much larger gear ratio. This gear ratio allowed for more precision in the brake, but still met the size constraints. The bearings chosen at this stage were simply thin faced axial thrust bearings, with no radial bearings. The base plate and side supports were curved to fit the shape of a shoe heel, and there were only some very small guide pieces to constrain the rotation of the brakes. This iteration can be seen in Figure 3.2 and is clearly an unfinished design.

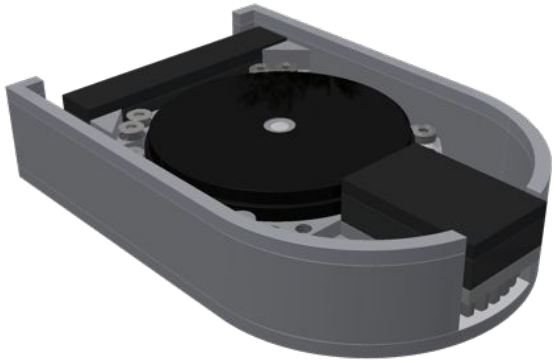

Figure 3.2: The first iteration of the design

After showing the design to the supervisors, some criticisms were made, which required some redesign.

First, the way the gears were set up, required the lead screw to pass through the rear brake asymmetrically, which would create a large torque on the screw, gear and base. This had to be redone somehow. The solution to this was to rethink the gear train, so that the gears could be centered directly underneath the brakes. This meant adding a set of intermediate gears to push the centers of the lead screws farther apart and allow for this geometry. This would in turn change the gear ratio and add more complexity, but it had to be done. In place of the 45-tooth gears that were originally there – see Figure 3.3 – two 20-tooth gears were added, and then two 25-tooth gears became the active gears. The gear ratio changed from 20:45 to 20:25, but after redoing the calculations, the change was not major.

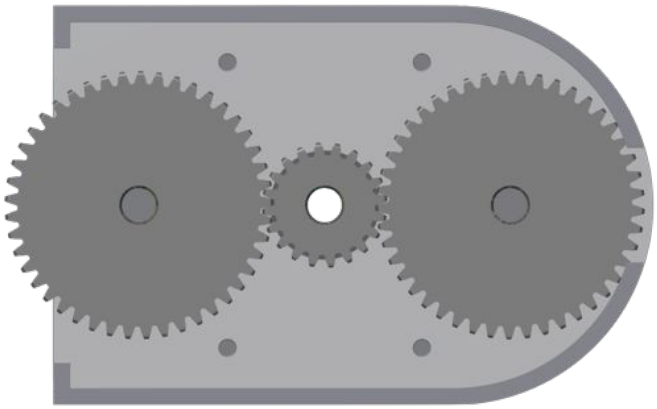

Figure 3.3: The gear train on the first iteration

Additional to the uneven loading of the brake was the consideration that there will be some tangential forces on the brakes that will cause a moment regardless of symmetry. This meant that the joints would be have a radial load, not just an axial load as I had assumed. The answer to this was to come up with some bearings that could handle this. Some sketches were made to model the forces and we came up with a setup that required two bearings and an extra bracket (Figure 3.4). After designing this, it was clear that it would be much too thick, and an alternative was considered. The alternative was to use an angular contact bearing that could handle both axial and radial loads. This proved to also be too thick.

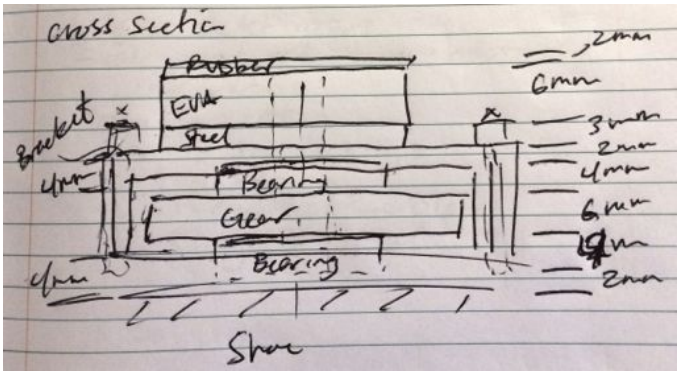


Figure 3.4: Preliminary sketch of bearings

The design that in the end would be successful involves one flanged radial ball bearing that fits in from the other side of the base plate and a needle roller bearing that fits around the radial bearing on top of the plate. As seen in Figure 3.5, the hub that runs through the

bearings is held in place with a circlip, or external retaining ring, which just keeps it from falling out due to gravity. With this setup, all the fits are slightly loose, so that the axial loads are transfered into the roller bearings and the radial loads into the ball bearings. This ensures that the system is not over-constrained.

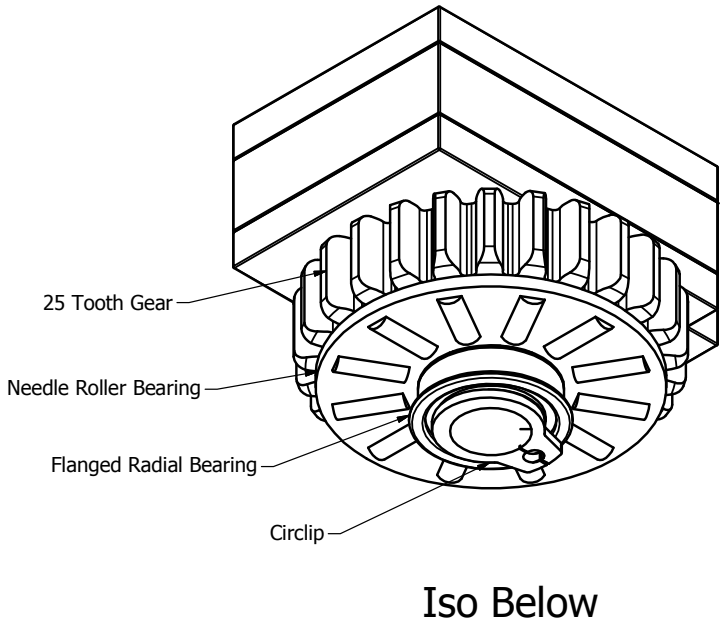


Figure 3.5: Drawing of the final bearing design for the rear brake

**Second Iteration** The second iteration involved adding guides for the brakes so that their rotation was constrained properly and that the friction between the brake plates and the surrounding components was not an issue. Custom aluminum pieces were designed to attach to the base plate and rest flush with the brake so that when it translated, it was guided by this part.

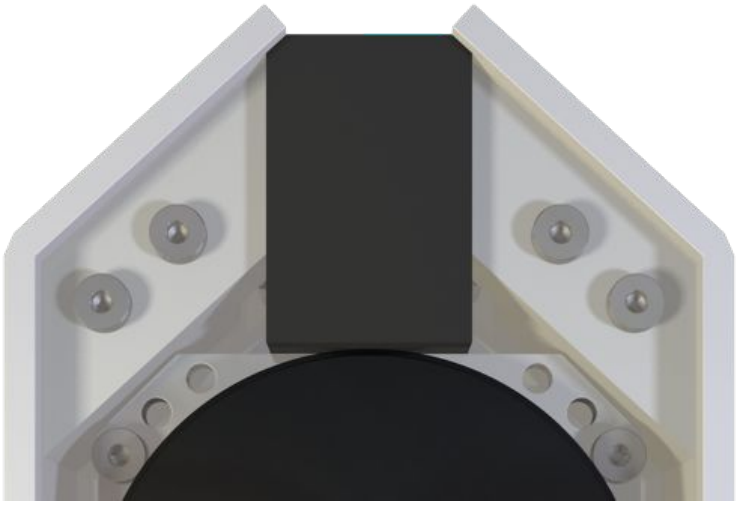

Figure 3.6: Second iteration showing addition of proper brake guides

In addition to this, the manufacturing methods were reexamined, and it became clear that the base plate and side supports would be difficult to machine into the curve shape, and this was an unnecessary feature. They were redesigned to just include one angle that would match the shape of of a shoe close enough to not be an issue, but make the machining and assembling much easier. Fasteners were also added in this iteration, as seen in Figure 3.7.

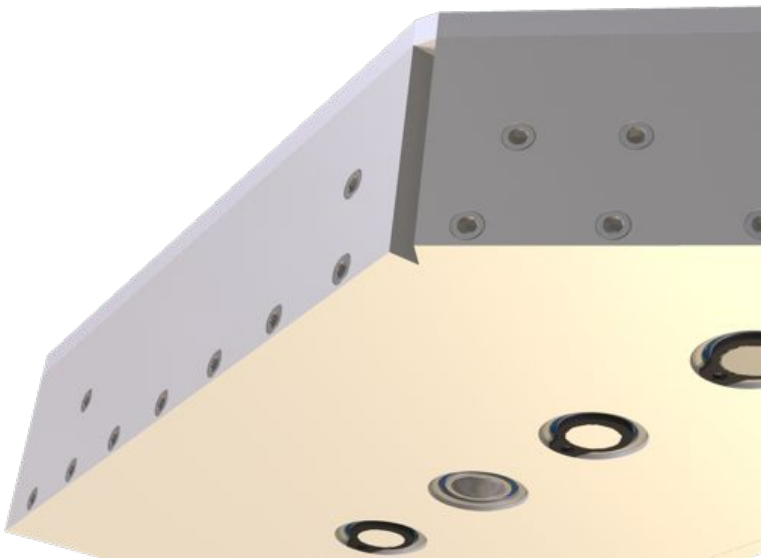

Figure 3.7: Second iteration showing the change in the base and sides

**Final Iteration** The final design made minor changes to the rear brake to address some issues that the heel strike would cause a large tangential force on the brake that would cause too much deformation towards the back of the device. To solve this, the supports and guides were changed so that the the leading edge of the heel would have a have a better balance of Teflon and rubber. This would add support when the shoe strikes the ground, so that it doesn't torque on the brake too much. Figures 3.8 and A.16 show this part of the final design.

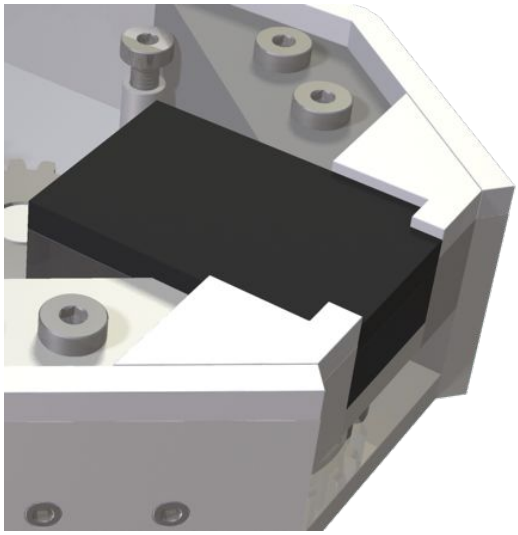

Figure 3.8: Final iteration with the change to the back brake

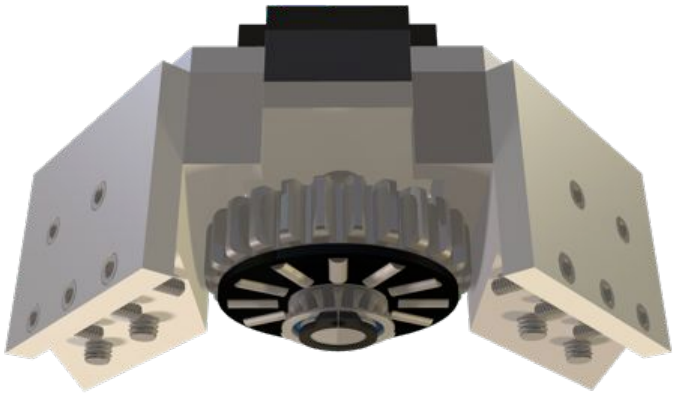

Figure 3.9: Final iteration showing the detail of the back brake

# 4

# Detailed Design

Figure 4.1: Final Detailed Design

The final design consists of five gears, five radial bearings, five circlips, two needle roller bearings, seven spacers, two hubs, two lead screws, seven steel plates, two EVA foam pieces, two rubber sheets, four PTFE sheets, three aluminum blocks, one motor, and thirty eight bolts. These parts make up the base plate, the supporting edges, the gear train, and front and rear brakes. The final detailed design takes into account the stresses on the brakes and edges, the friction in the gears, lead screws, and brakes, the material properties, the manufacturing of the parts, and the performance of the motor. After many calculations and a few iterations of design, the parts and materials are ready to be ordered. CAD renders in Appendix A show the many angles of the finished design, and drawings in Appendix B give details of how the device works.

# Parts & Materials

The device has been entirely designed with the choice of materials and parts in mind. When designing any device, it is important to always find sources for all the parts and materials that are required, as knowing what must be fabricated and what can be purchased weighs heavily on the success of the design. In the case of a mechanism such as the variable friction shoe surface device, sourcing components is especially difficult due to the size and load requirements. Some of the iterations of the design were made due entirely to the choice of parts. In the next section, the details of all the parts are laid out.

## Motor

The motor was chosen to be a pancake stepper motor, which is a hybrid brushless DC motor that moves in small increments of 1.8°. This style of motor runs off of DC voltage, has closed loop, yet very precise, rotation, and a high power density. The specific choice is the Moon's Industries 23HY9401 Pancake Super Flat 2-Phase stepper motor, that is only 9mm thick and a 55mm square profile (Appendix C.3). It weighs just 80 grams. The motor shaft is 6mm in diameter, which will be fit into the hubless drive gear.

## Gears

The gear train is made up of five gears; one drive gear with an intermediate gear on each side, and then an active gear outside each of those. The drive and intermediate gears are both 20-tooth gears, and the active gears on the outside are 25-tooth. This creates a gear ratio of 20:25 or 4:5, which gives the active gear less torque and slower motion. The gears being used come from Quality Transmission Components and are models SSAY1-20 and SSAY1-25. These models are steel, hubless, thin face spur gears and are only 6mm thick with pitch diameters of 20mm and 25mm respectively. They each weigh about 15 grams. Figure 4.2 shows the gear train from the bottom, with the plate and bearings removed.

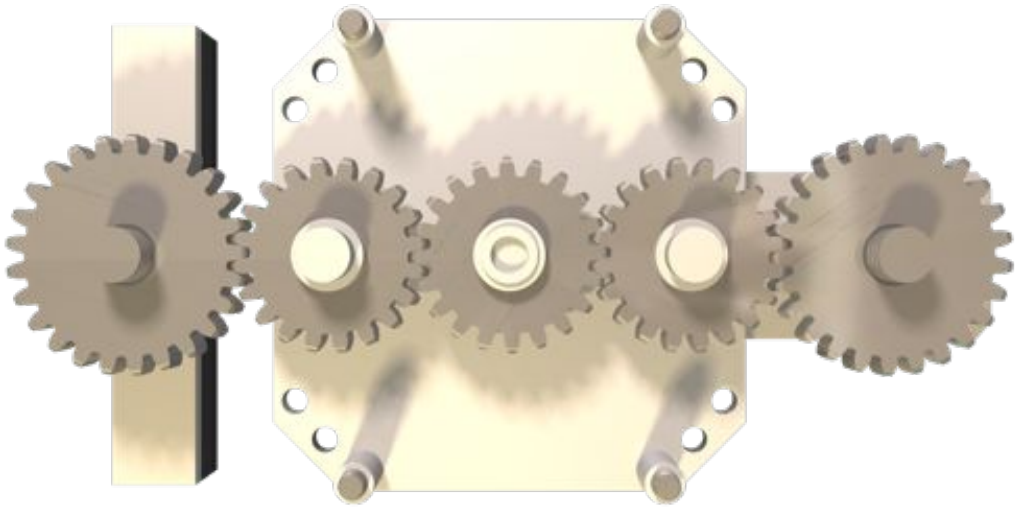

Figure 4.2: A look at the gear train

## Bearings

Two types of gears are used to allow movement with both axial and radial forces being exerted on the rotating parts. The two brakes are taking all the stress and most of that is in the axial direction, so they need bearings that can take this load. The axial load bearings chosen are NSK Thrust Needle Roller Bearings, with a very small thickness. They have an

I.D. of 10mm, O.D. of 24mm and thickness of 2mm, but can handle axial loads up to 7700N. These are the black bearings visible in Figure 4.3.

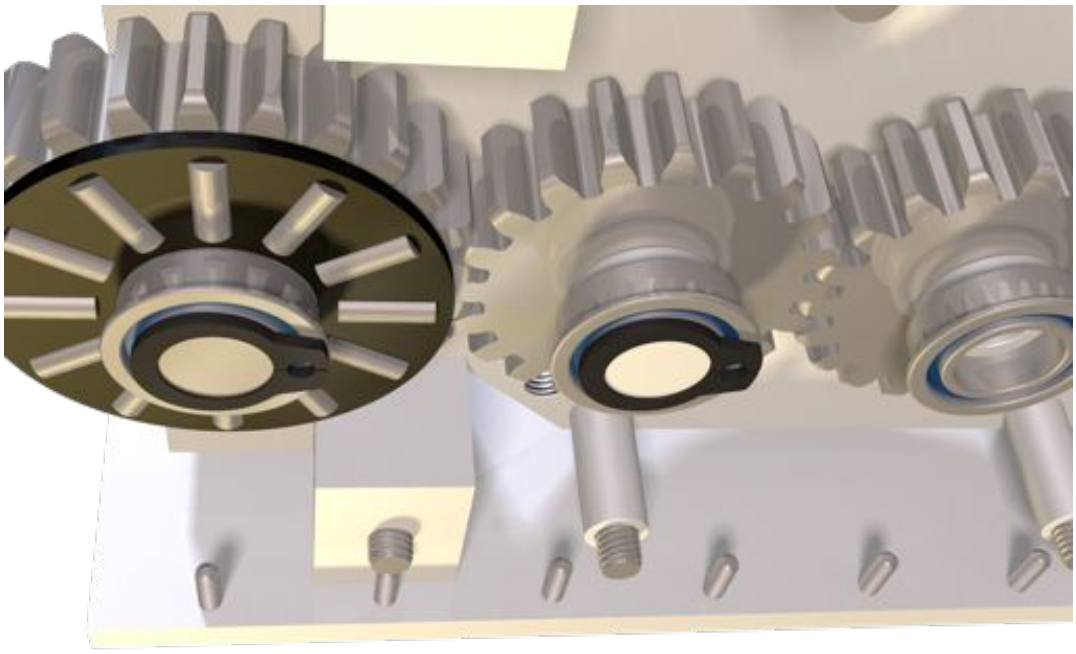

Figure 4.3: A close up of the bearings with the plate removed

The radial bearings are needed for all the gears to allow free rotation, and are chosen to be flanged so they can be attached from the other side of the base plate. Specifically, they are NSK Miniature Flanged Single-row Deep Groove Ball Bearings and have an I.D. of 6mm, O.D. of 10mm, and thickness of 3mm with the flange. They can still bear a radial load of up to 495N as shown in the spec sheet in Appendix C.2.

The shaft that runs through the radial bearings is then held into place by a 6mm circlip that can be found through McMaster. The Steel External Retaining Ring can take no load, but simply keeps the shaft from falling through. The bearings and circlip can be seen up close in Figure 4.4.

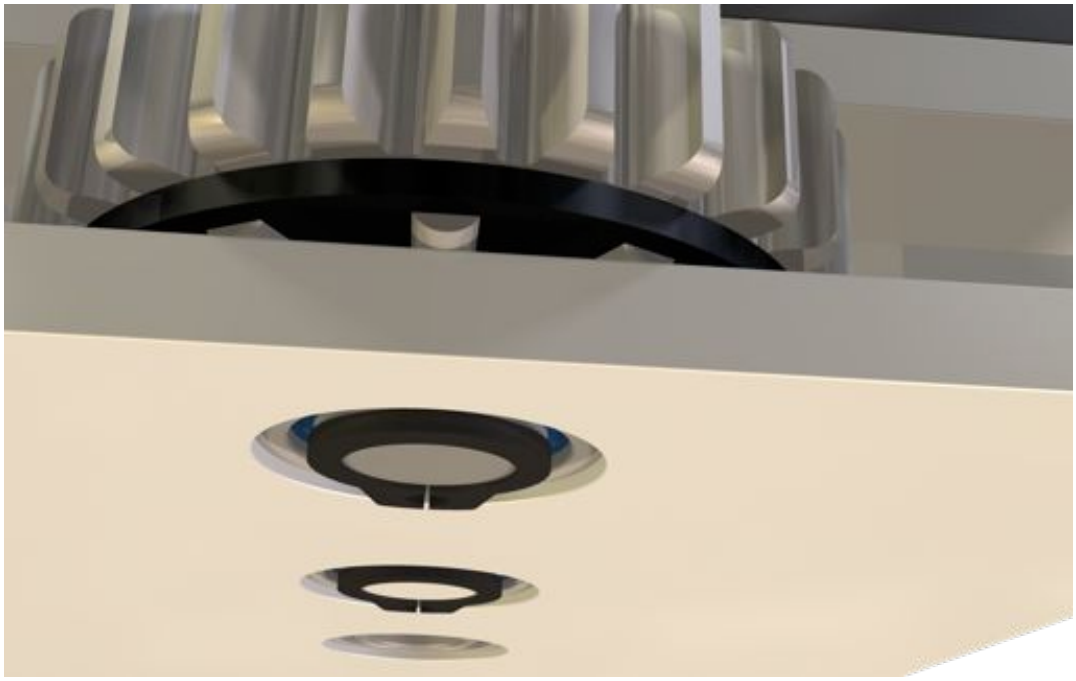

Figure 4.4: A closer look at the bearing and circlips

## Lead Screws

One lead screw on each brake is what drives them upwards and bears the load of the person. Fortunately, a 6mm lead screw is very strong, with a plastic nut typically good for 100lb, so with a custom, steel lead nut, the system should be robust enough to meet the requirements. The lead screw will be a Kerk Acme Rolled Stainless Steel Lead Screw with a 6mm diamater, cut to 20mm, with a special order lead nut, provided by Kerk as well. This combination should have a lead accuracy of .0001mm/mm, which means the resolution needed to attain our coefficients of friction will not be affected.

## Fasteners

All bolts were chosen to be stainless steel, metric, low head, socket cap screws for standardization and ease of assembly. Only one tool should be necessary to change all the bolts. All the bolts, except those that hold the side supports to the base are M3 bolts of varying length and are purchased from McMaster. The smaller bolts are M1.6 and are also found

on McMaster. No nuts were used, as all the screws should be threaded right into the base or corresponding part, which means that all the holes will have to be tapped.

The screws that hold the motor will need plastic spacers to lift the motor off the base plate the appropriate amount, and the three intermediate gears need thin spacers to align them with the active gears. These spacers are also standard parts available from McMaster, and will be ordered with the fasteners.

## Materials

The base plate, side supports, and brake guides will all be machined out of aluminum plates of varying thicknesses. The bottom plate and the side supports are made from a 3mm thick plate, while the brake guides will need to be machined from a block with a 20mm $\times$ 20mm profile.

The Teflon PTFE and gum rubber will be cut from a 3mm thick sheets and the EVA foam from a 6mm sheet. These are all standard materials and thicknesses that can be sourced from McMaster.

## Machining Methods

Some parts will need to be machined, and this has been considered in the design. The base plate is not too complicated, with angles cut from the corners and a few holes in a line down the middle. The side supports are simply rectangles with some holes drilled and countersunk. The only challenge is the brake guides, which involve some more advanced milling in the angles and cut-aways, but should still be able to be done in a conventional mill.

# 5

# Conclusion

After an initially easy decision on which concept to design, the minor details became the real extent of the design process. Making a device that fits into a shoe is no easy feat, and the the bulk of the research and design went into finding the right components and configurations to fit the size and load requirements. The final model reflects numerous calculations, hours of research, and many iterations of design.

The next step is to review the machine drawings and begin ordering parts and materials. This step can be done in early January so manufacturing can begin by the end of the month. Assembly should take about another couple weeks, and this leaves at least a month to test and redesign if necessary.

# Bibliography

[1] G. Millet, M. Otis, and J. R. Cooperstock, "Variable-friction devices for friction-controlled walking." Unpublished.

[2] V. Scott, L. Wagar, and S. Elliott, "Falls & related injuries among older canadians: fall-related hospitalizations & intervention initiatives," tech. rep., Public Health Agency of Canada, 2010.

[3] J. M. Hausdorff, D. A. Rios, and H. K. Edelberg, "Gait variability and fall risk in community-living older adults: A 1-year prospective study," *Archives of Physical Medicine and Rehabilitation*, vol. 82, no. 8, pp. 1050 – 1056, 2001.

[4] L.-W. Chu, I. Chi, and A. Chiu, "Incidence and predictors of falls in the chinese elderly," *Annals, Academy of Medicine, Singapore*, vol. 34, no. 1, pp. 60 – 72, 2005.

[5] H. Luukinen, K. Koski, L. Hiltunen, and S.-L. Kivela, "Incidence rate of falls in an aged population in northern finland," *Journal of Clinical Epidemiology*, vol. 47, no. 8, pp. 843 – 850, 1994.

[6] A. Roberts and J. Richardson, "Interface study of rubber-ice friction," *Wear*, vol. 67, no. 1, pp. 55 – 69, 1981.

# Appendix A

# CAD Renders

Figure A.1: Isometric overview

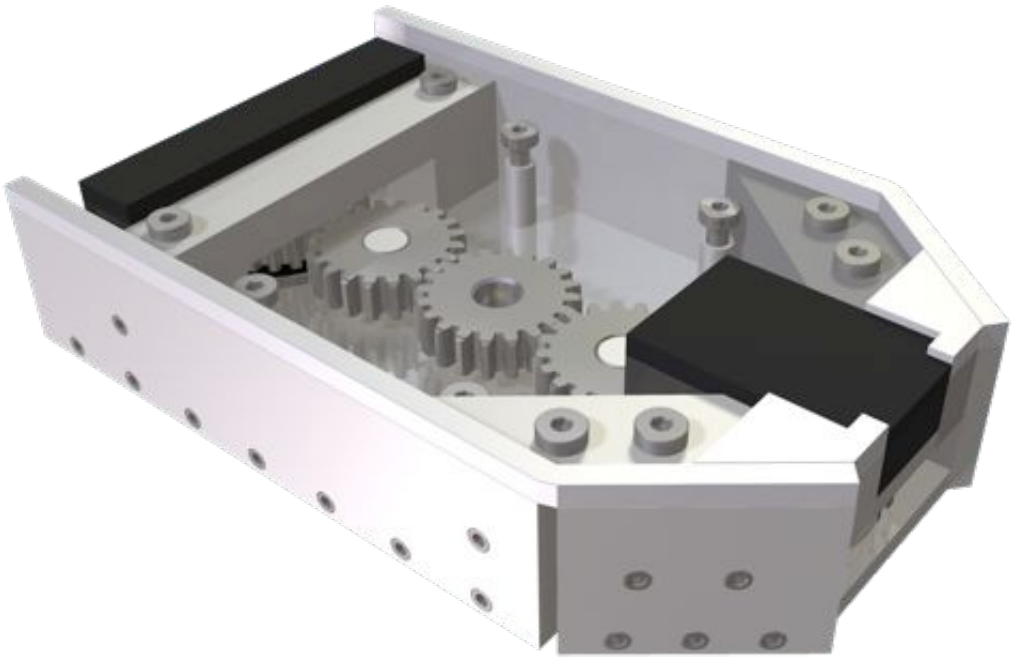

Figure A.2: Isometric overview without the motor

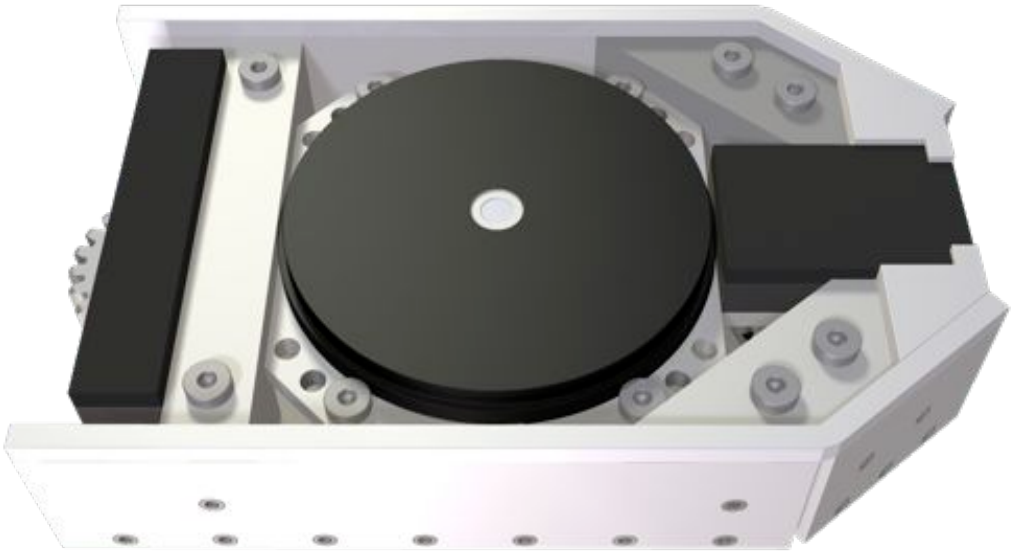

Figure A.3: Overview of the mechanism from the side

Figure A.4: View of the side with the supports removed for viewing

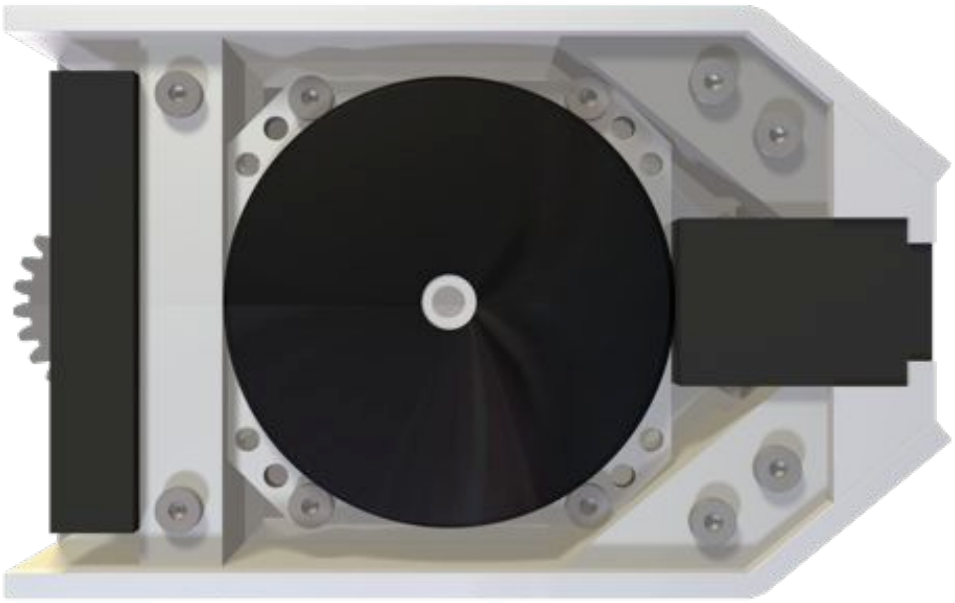

Figure A.5: Top view

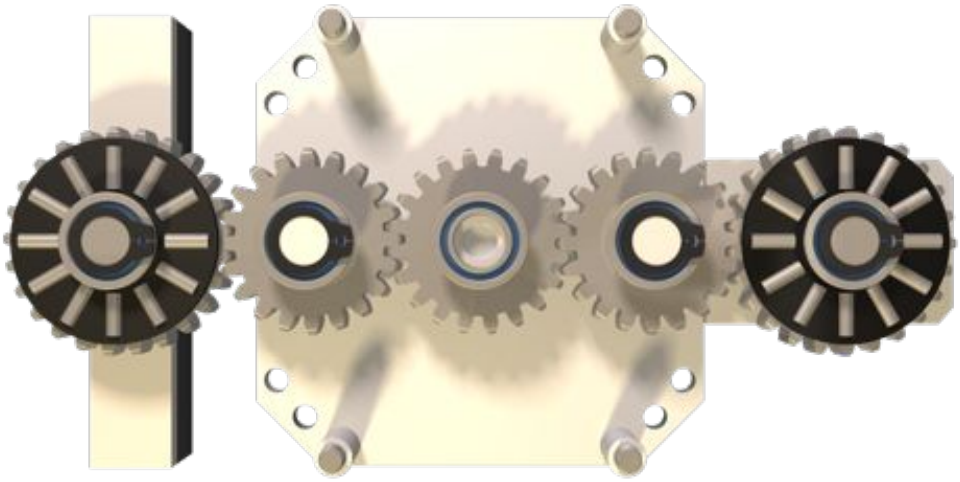

Figure A.6: Bottom with bearings visible

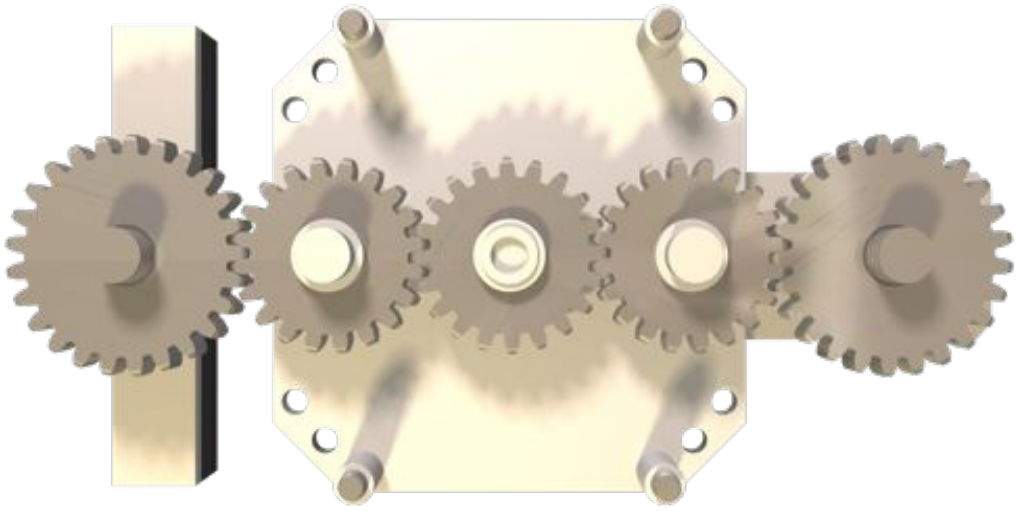

Figure A.7: Bottom with no bearings

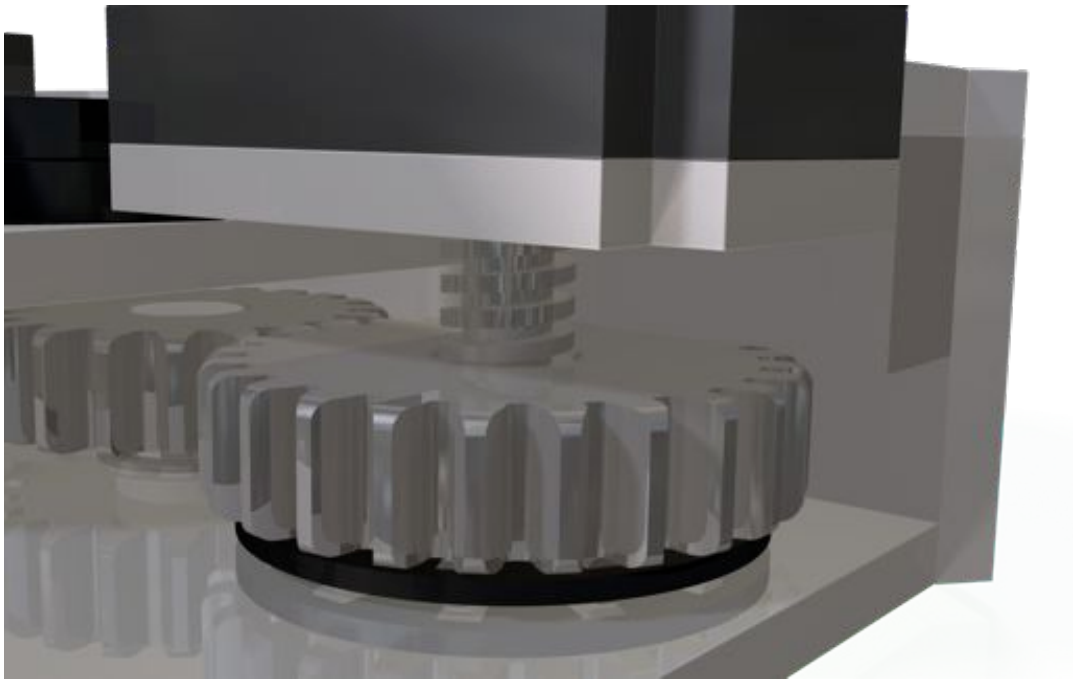

Figure A.8: Close up of back brake

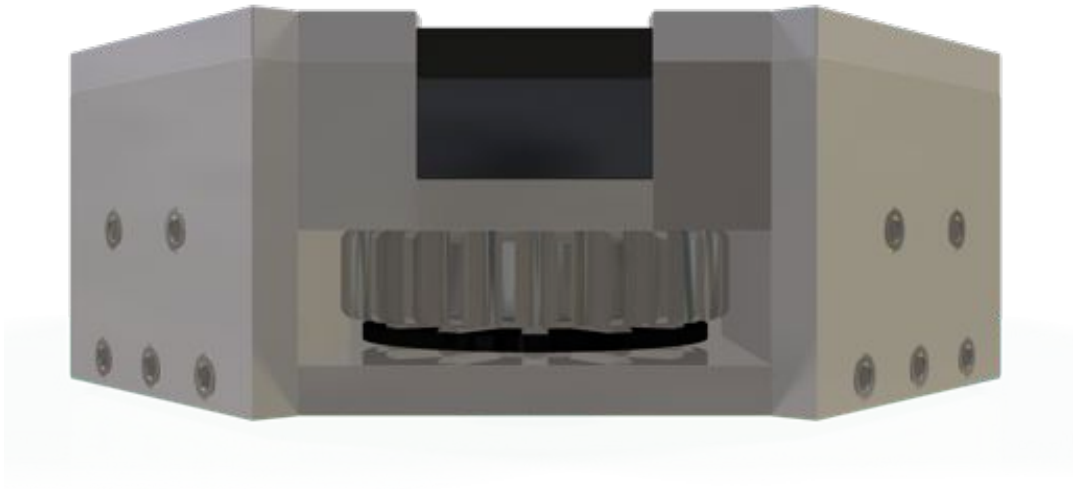

Figure A.9: Back brake in down position

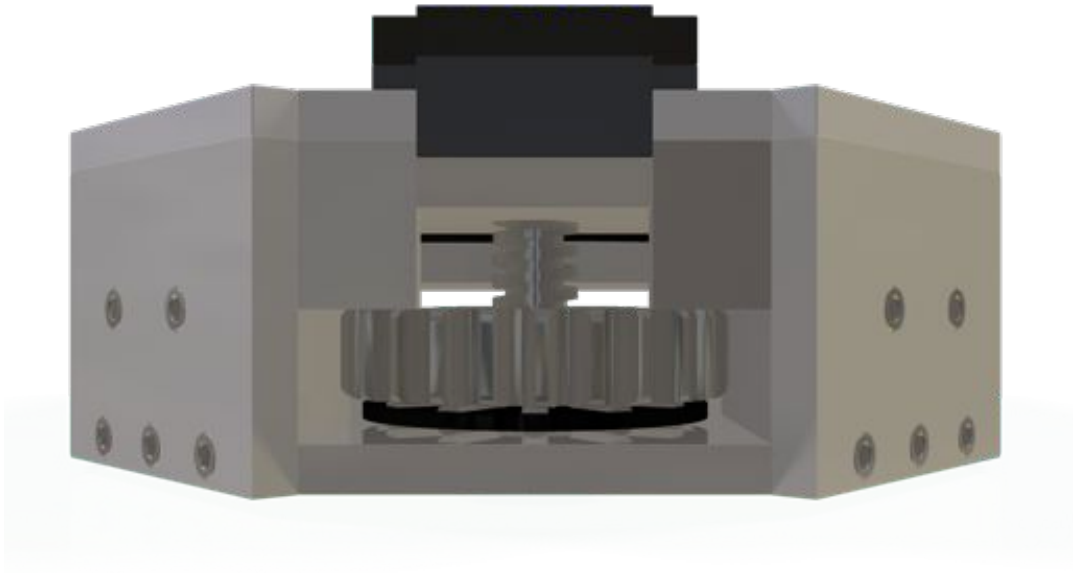

Figure A.10: Back brake in up position

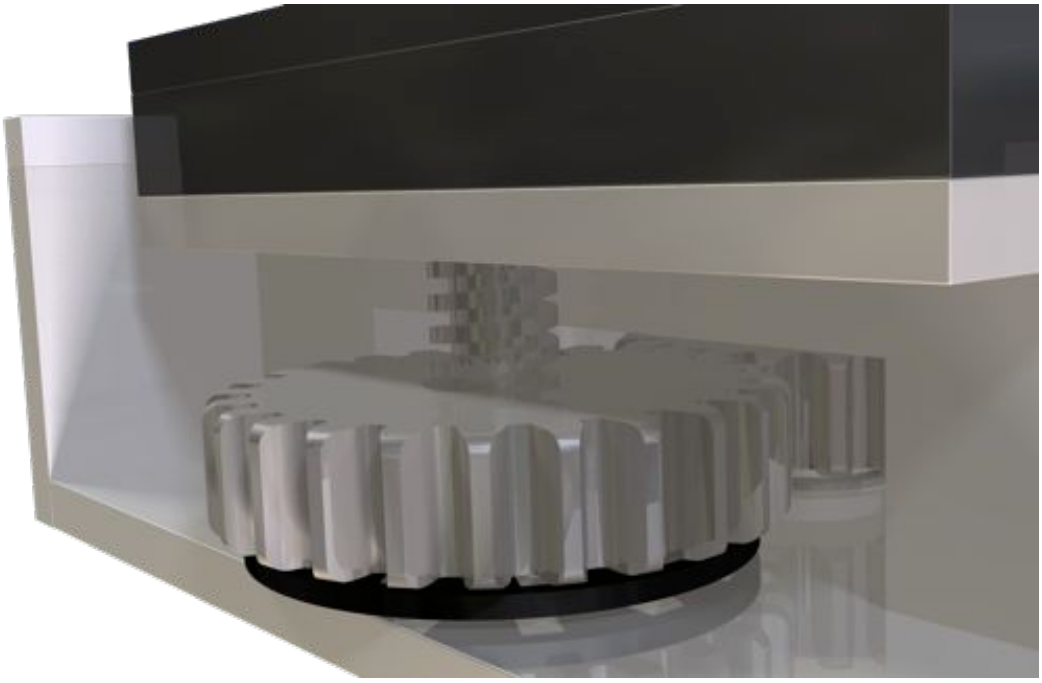

Figure A.11: Close up of front brake

Figure A.12: Front brake in down position

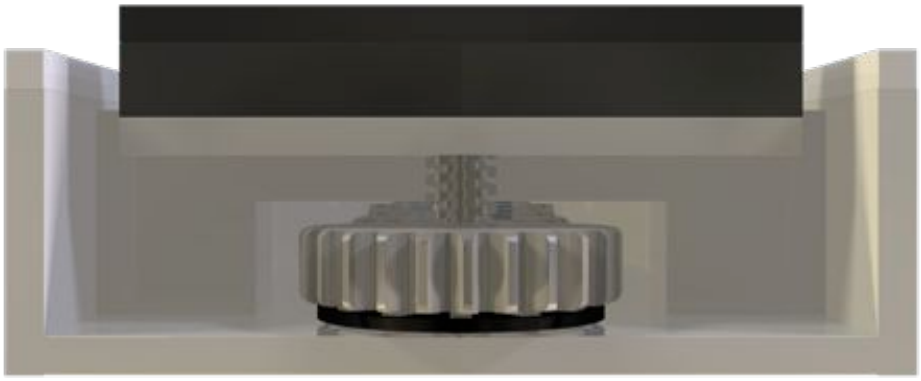

Figure A.13: Front brake in up position

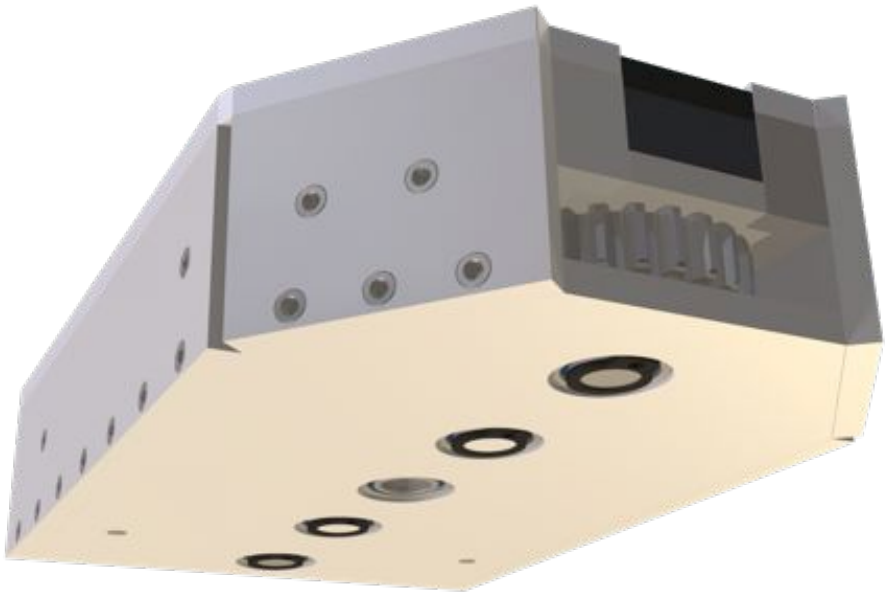

Figure A.14: Isometric view from below

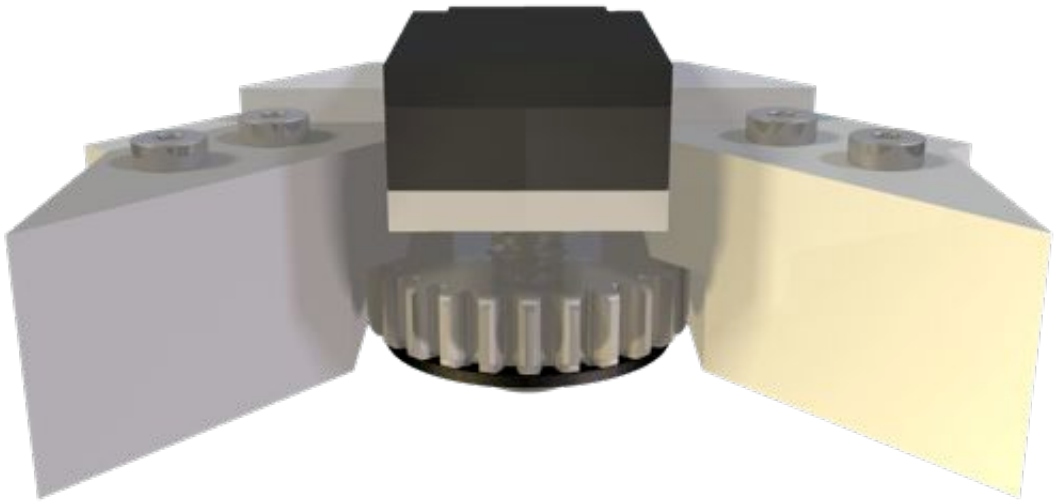

Figure A.15: The rear brake system with brake guides

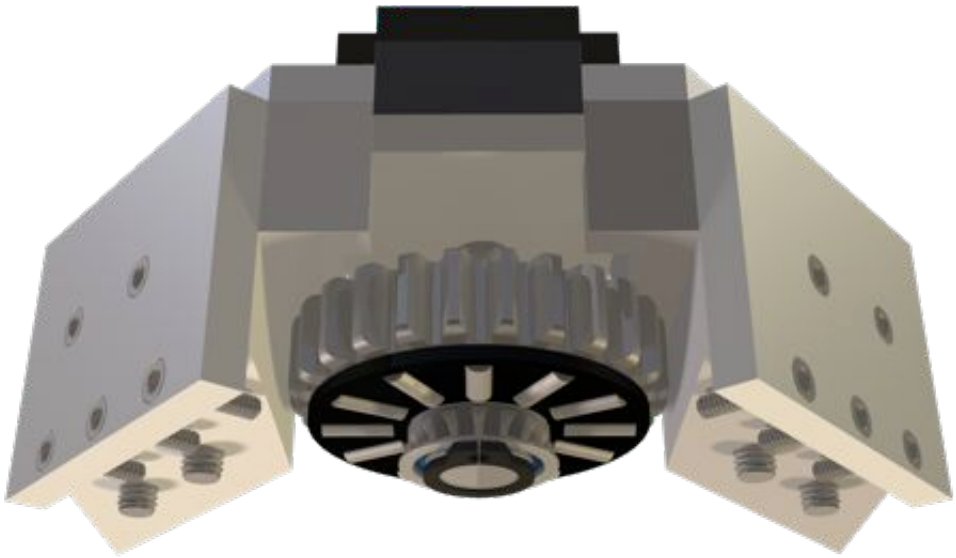

Figure A.16: The rear brake system from the back

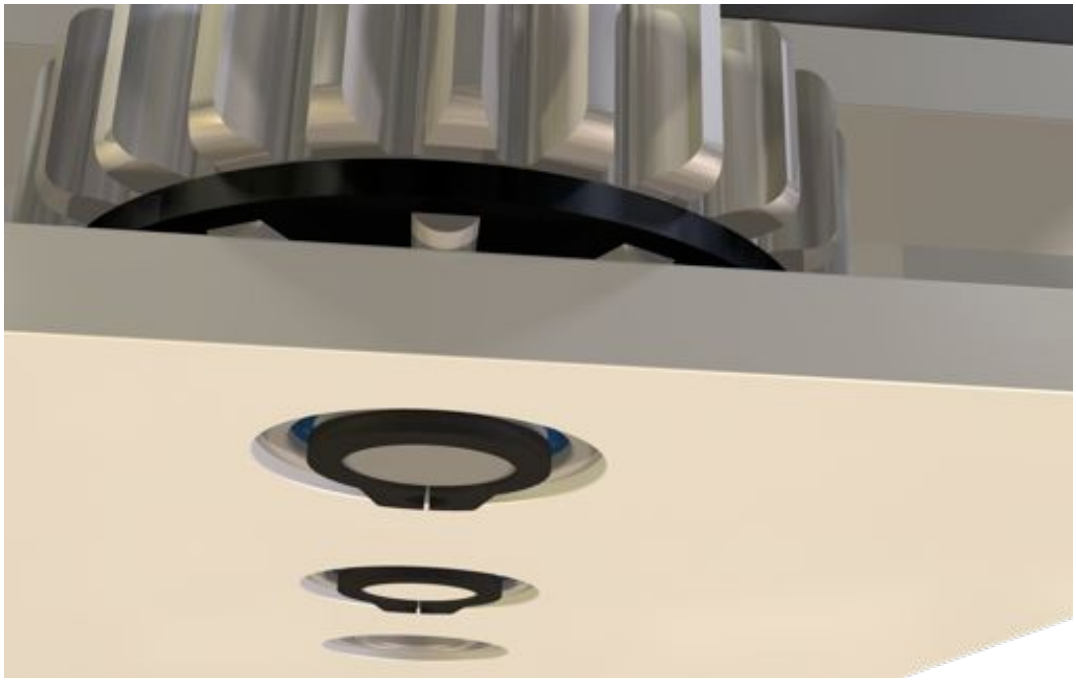

Figure A.17: A close up of the bearings, gears, and circlip

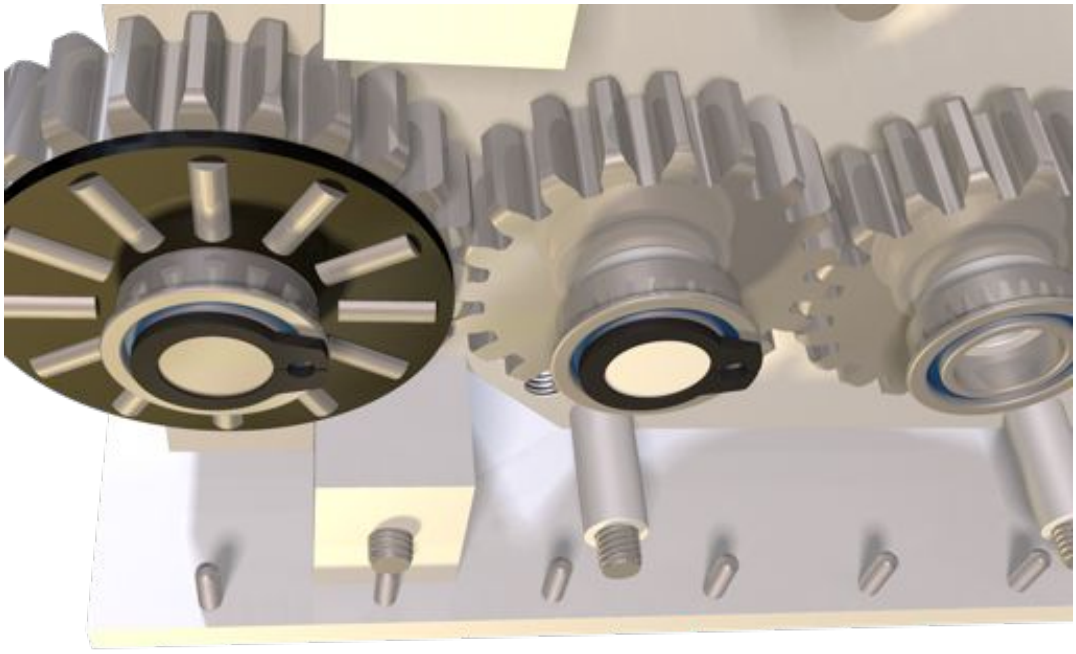

Figure A.18: A close up of the bearings, circlip, and gears, with the plate removed

# Appendix B

# Machine Drawings

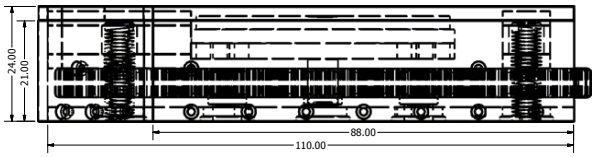


Side

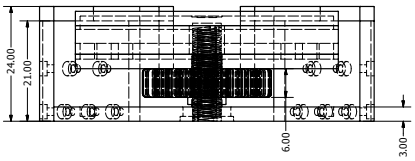


Front

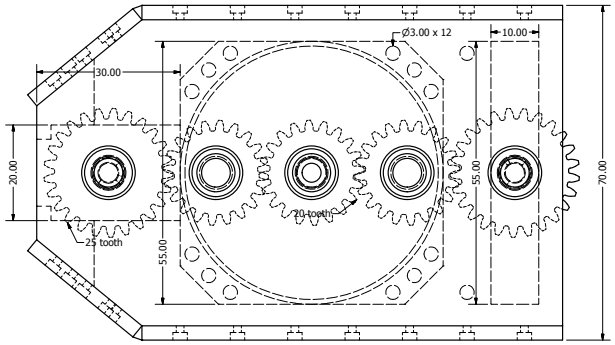


Top

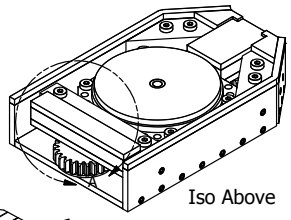

Iso Above

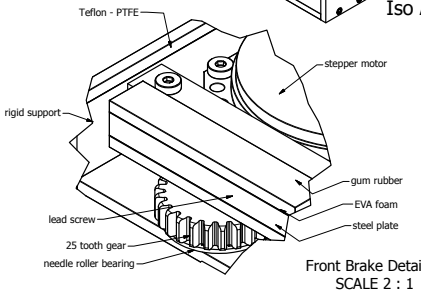


Front Brake Detail A
SCALE 2 : 1

| | | | |
|---|---|---|---|
| DRAWN Michael King | 12/4/2013 | McGill University - Mechanical Engineering | |
| CHECKED | | TITLE | |
| QA | | Variable Friction Shoe Mechanism | |
| MFG | | | |
| APPROVED | | SIZE C | DWG NO MASTER-ASSEMBLY REV |
| UNITS: mm | | SCALE 2:1 | SHEET 1 OF 1 |

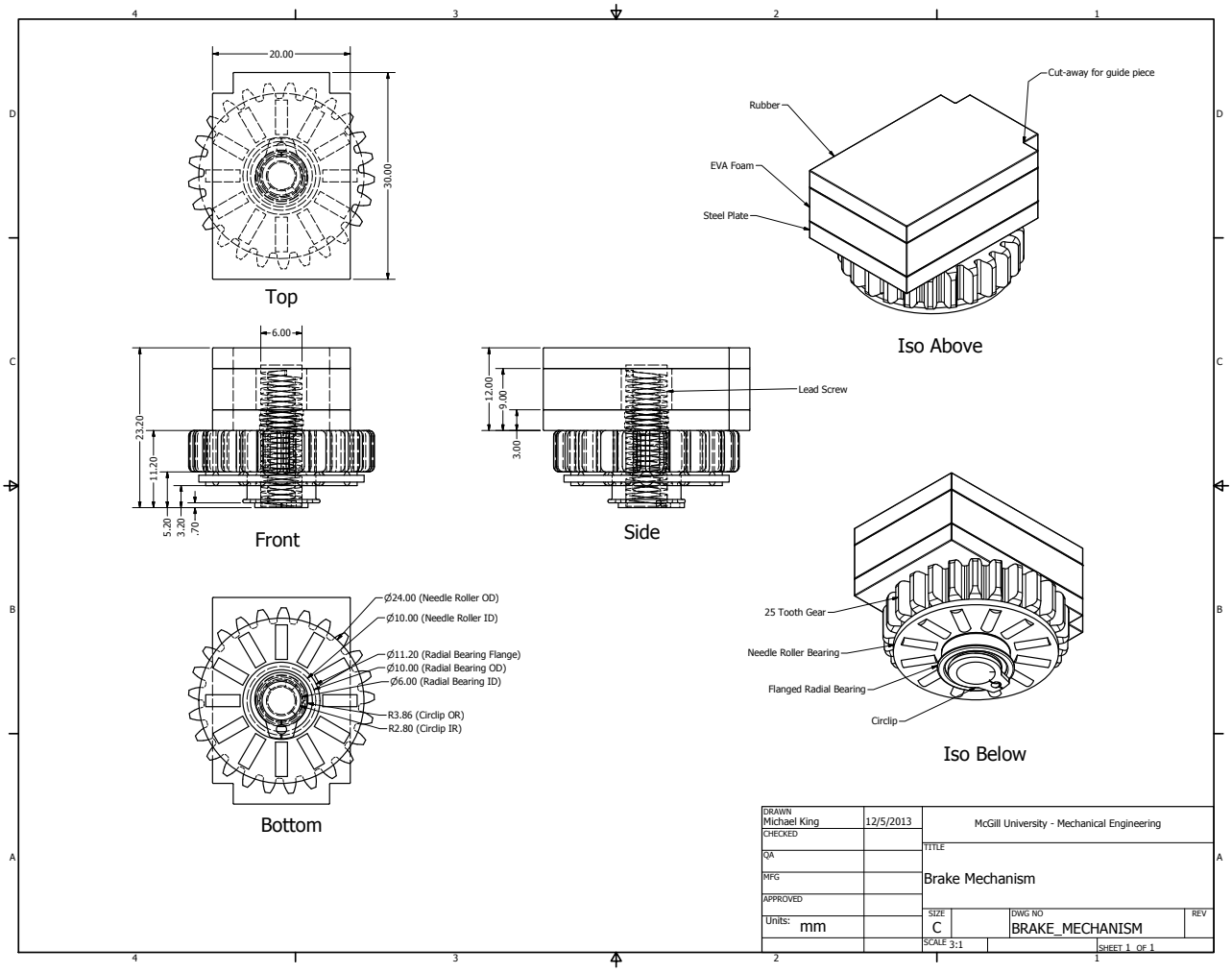


| | | |
|---|---|---|
| DRAWN Michael King | 12/5/2013 | McGill University - Mechanical Engineering |
| CHECKED | | |
| QA | | TITLE: Brake Mechanism |
| MFG | | |
| APPROVED | | |
| Units: mm | | SIZE C; DWG NO BRAKE_MECHANISM; REV |
| | | SCALE 3:1; SHEET 1 OF 1 |

# Appendix C

# Product Specifications

| Boundary Dimensions (mm) | | | Basic Load Ratings (N) | | Limiting Speeds ($min^{-1}$) | Bearing Numbers | Bearing Numbers of Matching Bearing Rings | | | | | NSKHPS |
|---|---|---|---|---|---|---|---|---|---|---|---|---|
| $D_{c1}$,$D_{p1}$ | $D_c$,$D_p$ | $D_w$ | $C_a$ | $C_{0a}$ | Oil | | $s$=1.0 | $s$=1.5 | $s$=2.0 | $s$=2.5 | $s$=3.0 | |
| **10** | 24 | 2 | 7750 | 23000 | 17000 | **FNTA-1024** | FTRA-1024 | FTRB-1024 | FTRC-1024 | - | - | |
| **12** | 26 | 2 | 8350 | 26300 | 16000 | **FNTA-1226** | FTRA-1226 | FTRB-1226 | FTRC-1226 | - | - | |
| **15** | 28 | 2 | 7950 | 25800 | 15000 | **FNTA-1528** | FTRA-1528 | FTRB-1528 | FTRC-1528 | FTRD-1528 | FTRE-1528 | |
| **16** | 29 | 2 | 8200 | 27100 | 14000 | **FNTA-1629** | FTRA-1629 | FTRB-1629 | FTRC-1629 | FTRD-1629 | FTRE-1629 | |
| **17** | 30 | 2 | 8400 | 28400 | 14000 | **FNTA-1730** | FTRA-1730 | FTRB-1730 | FTRC-1730 | FTRD-1730 | FTRE-1730 | |
| **18** | 31 | 2 | 8600 | 29700 | 13000 | **FNTA-1831** | FTRA-1831 | FTRB-1831 | FTRC-1831 | FTRD-1831 | FTRE-1831 | |
| **20** | 35 | 2 | 11900 | 47000 | 12000 | **FNTA-2035** | FTRA-2035 | FTRB-2035 | FTRC-2035 | FTRD-2035 | FTRE-2035 | |
| **25** | 42 | 2 | 14800 | 66000 | 9500 | **FNTA-2542** | FTRA-2542 | FTRB-2542 | FTRC-2542 | FTRD-2542 | FTRE-2542 | |
| **30** | 47 | 2 | 16500 | 79000 | 8500 | **FNTA-3047** | FTRA-3047 | FTRB-3047 | FTRC-3047 | FTRD-3047 | FTRE-3047 | |
| **35** | 52 | 2 | 17300 | 88000 | 8000 | **FNTA-3552** | FTRA-3552 | FTRB-3552 | FTRC-3552 | FTRD-3552 | FTRE-3552 | |
| **40** | 60 | 3 | 26900 | 122000 | 6700 | **FNTA-4060** | FTRA-4060 | FTRB-4060 | FTRC-4060 | FTRD-4060 | FTRE-4060 | |
| **45** | 65 | 3 | 28700 | 137000 | 6300 | **FNTA-4565** | FTRA-4565 | FTRB-4565 | FTRC-4565 | FTRD-4565 | FTRE-4565 | |
| **50** | 70 | 3 | 30500 | 152000 | 5600 | **FNTA-5070** | FTRA-5070 | FTRB-5070 | FTRC-5070 | FTRD-5070 | FTRE-5070 | |
| **55** | 78 | 3 | 37000 | 201000 | 5300 | **FNTA-5578** | FTRA-5578 | FTRB-5578 | FTRC-5578 | FTRD-5578 | FTRE-5578 | |
| **60** | 85 | 3 | 43000 | 252000 | 4800 | **FNTA-6085** | FTRA-6085 | FTRB-6085 | FTRC-6085 | FTRD-6085 | FTRE-6085 | |
| **65** | 90 | 3 | 45500 | 274000 | 4500 | **FNTA-6590** | FTRA-6590 | FTRB-6590 | FTRC-6590 | FTRD-6590 | FTRE-6590 | |
| **70** | 95 | 4 | 59000 | 320000 | 4300 | **FNTA-7095** | FTRA-7095 | FTRB-7095 | FTRC-7095 | FTRD-7095 | FTRE-7095 | |
| **75** | 100 | 4 | 60000 | 335000 | 4000 | **FNTA-75100** | FTRA-75100 | FTRB-75100 | FTRC-75100 | FTRD-75100 | FTRE-75100 | |
| **80** | 105 | 4 | 63000 | 365000 | 3800 | **FNTA-80105** | FTRA-80105 | FTRB-80105 | FTRC-80105 | FTRD-80105 | FTRE-80105 | |
| **85** | 110 | 4 | 64500 | 380000 | 3600 | **FNTA-85110** | FTRA-85110 | FTRB-85110 | FTRC-85110 | FTRD-85110 | FTRE-85110 | |
| **90** | 120 | 4 | 80000 | 515000 | 3400 | **FNTA-90120** | FTRA-90120 | FTRB-90120 | FTRC-90120 | FTRD-90120 | FTRE-90120 | |
| **100** | 135 | 4 | 98500 | 695000 | 3000 | **FNTA-100135** | FTRA-100135 | FTRB-100135 | FTRC-100135 | FTRD-100135 | FTRE-100135 | |



Figure C.1: Specifications of the NSK needle roller bearings

# メートル系　フランジ付き単列深溝玉軸受
## Single-row deep groove ball bearings with flanged outer ring (Metric series)

**F600** 形
**F600,MF**
**MF** 形
内径　5～9mm
**Bore diameter 5～9mm**

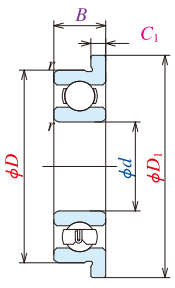

開放形
Open type

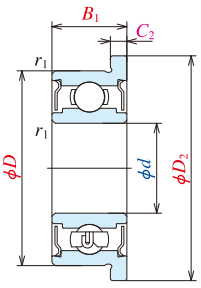

シールド形
Shielded type
ZZ

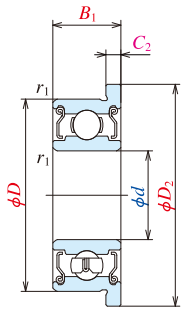

シールド形
Shielded type
ZZ1

| 呼び番号 Bearing numbers | | | 主要寸法（mm） Boundary dimensions | | | | | | | | | | 基本定格荷重 Basic load ratings | | | |
|---|---|---|---|---|---|---|---|---|---|---|---|---|---|---|---|---|
| | | | | | | | | | | | | | （N） | | {kgf} | |
| 開放形 Open | シールド形 Shielded | シールド形 Sealed | $d$ | $D$ | $D_1$ | $D_2$ | $B$ | $B_1$ | $C_1$ | $C_2$ | $r$ 最小 min | $r_1$ 最小 min | $C_r$ | $C_{or}$ | $C_r$ | $C_{or}$ |
| **MF85** | — | — — | **5** | 8 | 9.2 | — | 2 | — | 0.6 | — | 0.10 | — | 310 | 120 | 31 | 12 |
| — | **MF85ZZ** | — — | | 8 | — | 9.2 | — | 2.5 | — | 0.6 | — | 0.10 | 278 | 131 | 28 | 13 |
| **MF95** | **MF95ZZ** | — — | | 9 | 10.2 | 10.2 | 2.5 | 3 | 0.6 | 0.6 | 0.15 | 0.15 | 430 | 168 | 44 | 17 |
| **MF105** | **MF105ZZ** | — — | | 10 | 11.2 | 11.6 | 3 | 4 | 0.6 | 0.8 | 0.15 | 0.15 | 430 | 168 | 44 | 17 |
| **F685** | **F685ZZ** | — — | | 11 | 12.5 | 12.5 | 3 | 5 | 0.8 | 1 | 0.15 | 0.15 | 715 | 281 | 73 | 29 |
| **F695** | **F695ZZ1** | VV DD | | 13 | 15 | 15 | 4 | 4 | 1 | 1 | 0.20 | 0.20 | 1080 | 430 | 110 | 44 |
| **F605** | **F605ZZ** | — DD | | 14 | 16 | 16 | 5 | 5 | 1 | 1 | 0.20 | 0.20 | 1330 | 505 | 135 | 52 |
| **F625** | **F625ZZ1** | VV DD | | 16 | 18 | 18 | 5 | 5 | 1 | 1 | 0.30 | 0.30 | 1730 | 670 | 177 | 68 |
| **F635** | **F635ZZ1** | VV DD | | 19 | 22 | 22 | 6 | 6 | 1.5 | 1.5 | 0.30 | 0.30 | 2340 | 885 | 238 | 90 |
| **MF106** | **MF106ZZ1** | — — | **6** | 10 | 11.2 | 11.2 | 2.5 | 3 | 0.6 | 0.6 | 0.15 | 0.10 | 495 | 218 | 51 | 22 |
| **MF126** | **MF126ZZ** | — DD | | 12 | 13.2 | 13.6 | 3 | 4 | 0.6 | 0.8 | 0.20 | 0.15 | 715 | 292 | 73 | 30 |
| **F686A** | **F686AZZ1** | VV DD | | 13 | 15 | 15 | 3.5 | 5 | 1 | 1.1 | 0.15 | 0.15 | 1080 | 440 | 110 | 45 |
| **F696** | **F696ZZ1** | VV DD | | 15 | 17 | 17 | 5 | 5 | 1.2 | 1.2 | 0.20 | 0.20 | 1730 | 670 | 177 | 68 |
| **F606** | **F606ZZ** | VV DD | | 17 | 19 | 19 | 6 | 6 | 1.2 | 1.2 | 0.30 | 0.30 | 2260 | 835 | 231 | 85 |
| **F626** | **F626ZZ1** | VV DD | | 19 | 22 | 22 | 6 | 6 | 1.5 | 1.5 | 0.30 | 0.30 | 2340 | 885 | 238 | 90 |
| **F636** | **F636ZZ** | VV DD | | 22 | 25 | 25 | 7 | 7 | 1.5 | 1.5 | 0.30 | 0.30 | 3300 | 1370 | 335 | 140 |
| **MF117** | **MF117ZZ** | — — | **7** | 11 | 12.2 | 12.2 | 2.5 | 3 | 0.6 | 0.6 | 0.15 | 0.10 | 455 | 201 | 47 | 21 |
| **MF137** | **MF137ZZ** | — — | | 13 | 14.2 | 14.6 | 3 | 4 | 0.6 | 0.8 | 0.20 | 0.15 | 540 | 276 | 55 | 28 |
| **F687** | **F687ZZ1** | VV DD | | 14 | 16 | 16 | 3.5 | 5 | 1 | 1.1 | 0.15 | 0.15 | 1170 | 510 | 120 | 52 |
| **F697** | **F697ZZ1** | VV DD | | 17 | 19 | 19 | 5 | 5 | 1.2 | 1.2 | 0.30 | 0.30 | 1610 | 710 | 164 | 73 |
| **F607** | **F607ZZ1** | VV DD | | 19 | 22 | 22 | 6 | 6 | 1.5 | 1.5 | 0.30 | 0.30 | 2340 | 885 | 238 | 90 |
| **F627** | **F627ZZ** | VV DD | | 22 | 25 | 25 | 7 | 7 | 1.5 | 1.5 | 0.30 | 0.30 | 3300 | 1370 | 335 | 140 |
| **MF128** | **MF128ZZ1** | VV DD | **8** | 12 | 13.2 | 13.6 | 2.5 | 3.5 | 0.6 | 0.8 | 0.15 | 0.10 | 545 | 274 | 56 | 28 |
| **MF148** | **MF148ZZ** | VV DD | | 14 | 15.6 | 15.6 | 3.5 | 4 | 0.8 | 0.8 | 0.20 | 0.15 | 820 | 385 | 83 | 39 |
| **F688A** | **F688AZZ1** | VV DD | | 16 | 18 | 18 | 4 | 5 | 1 | 1.1 | 0.20 | 0.20 | 1610 | 710 | 164 | 73 |
| **F698** | **F698ZZ1** | VV DD | | 19 | 22 | 22 | 6 | 6 | 1.5 | 1.5 | 0.30 | 0.30 | 2240 | 910 | 228 | 93 |
| **F689** | **F689ZZ** | VV DD | **9** | 17 | 19 | 19 | 4 | 5 | 1 | 1.1 | 0.20 | 0.20 | 1330 | 665 | 136 | 68 |

注　（*1）外径、内径の実寸法を示します。
Notes　Actual dimensions of bore and outside diameter only.
（2）ステンレス品の基本動定格荷重は0.85掛けが目安となります。
The rough standard of basic dynamic load rating for stainless products would be15% less than the value appeared in the list.





Figure C.2: Specifications of the NSK radial flanged bearings

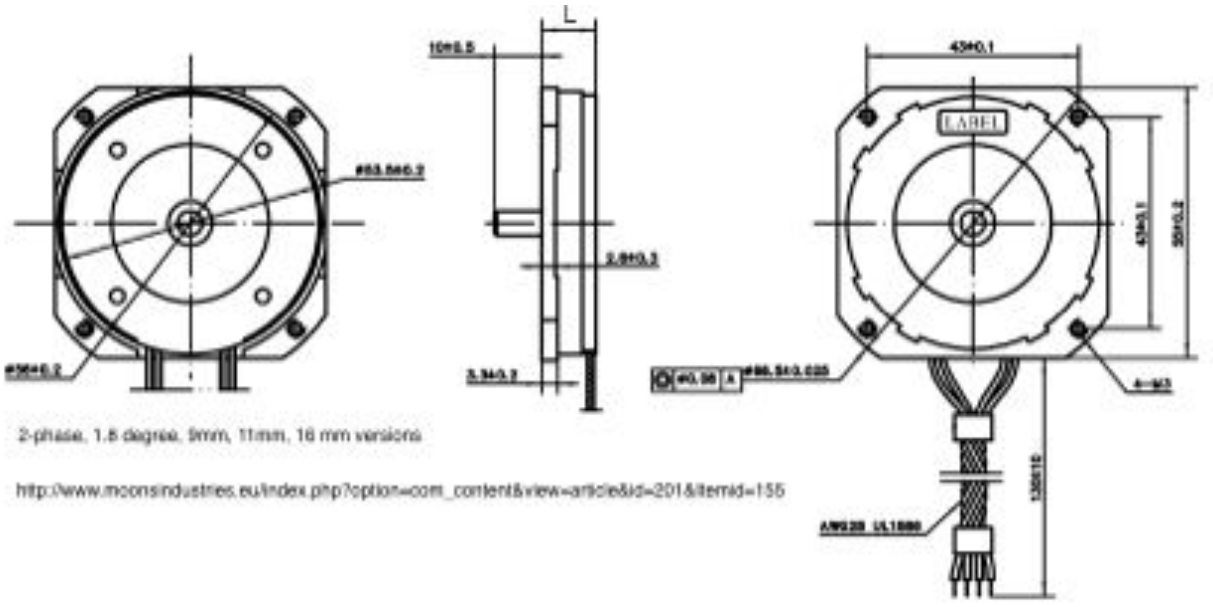


Figure C.3: Moon's Industries 23HY9401 Pancake Super Flat 2-Phase Stepper Motor

# Appendix D

# Photos

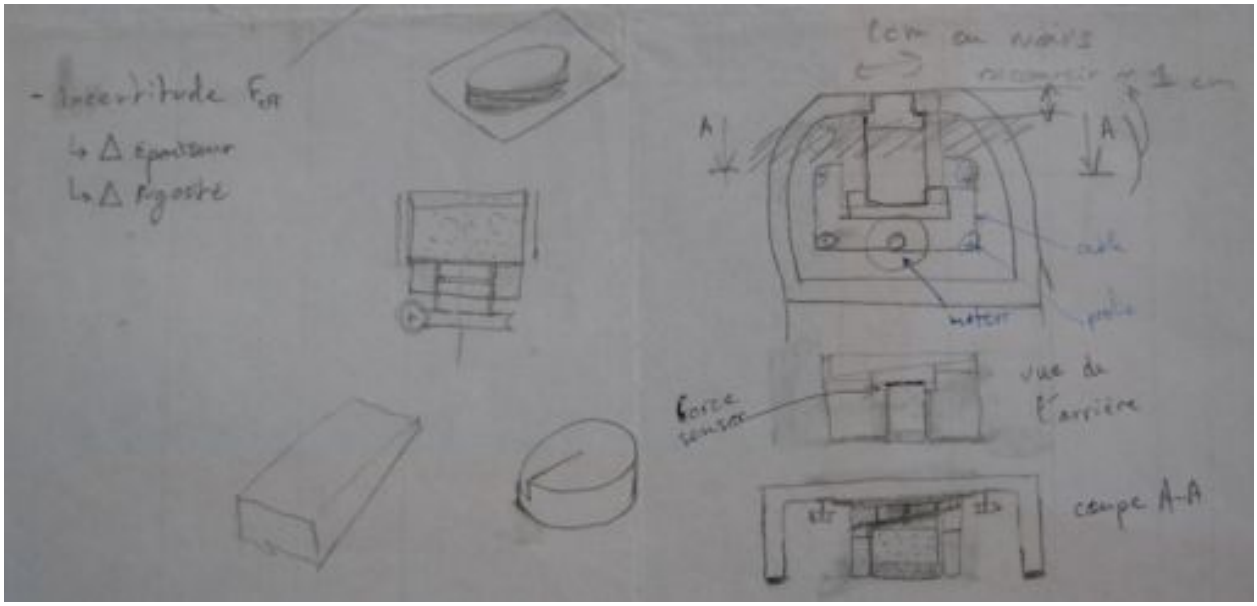


Figure D.1: Very preliminary sketch by G. Millet

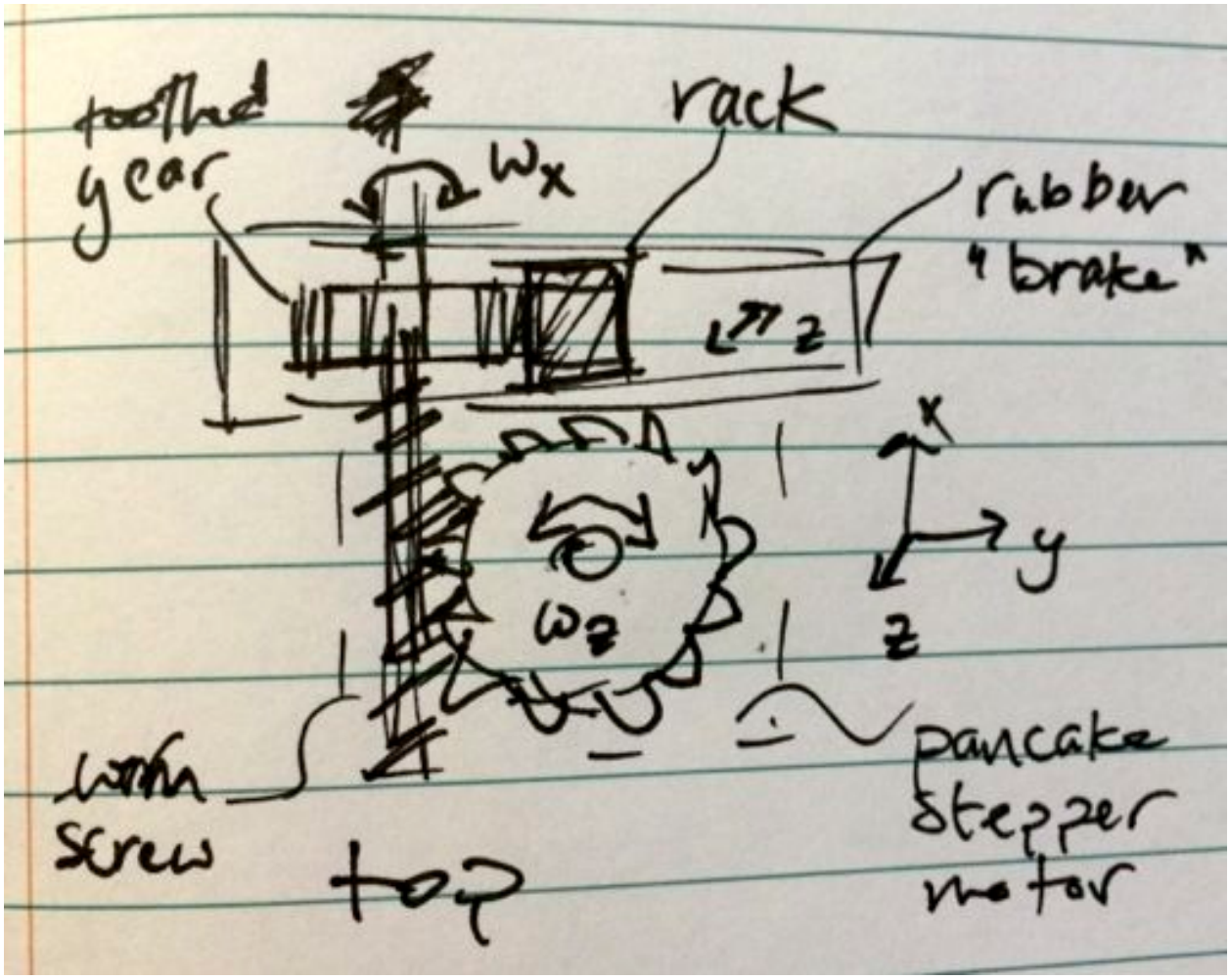


Figure D.2: Preliminary sketch of worm gear idea

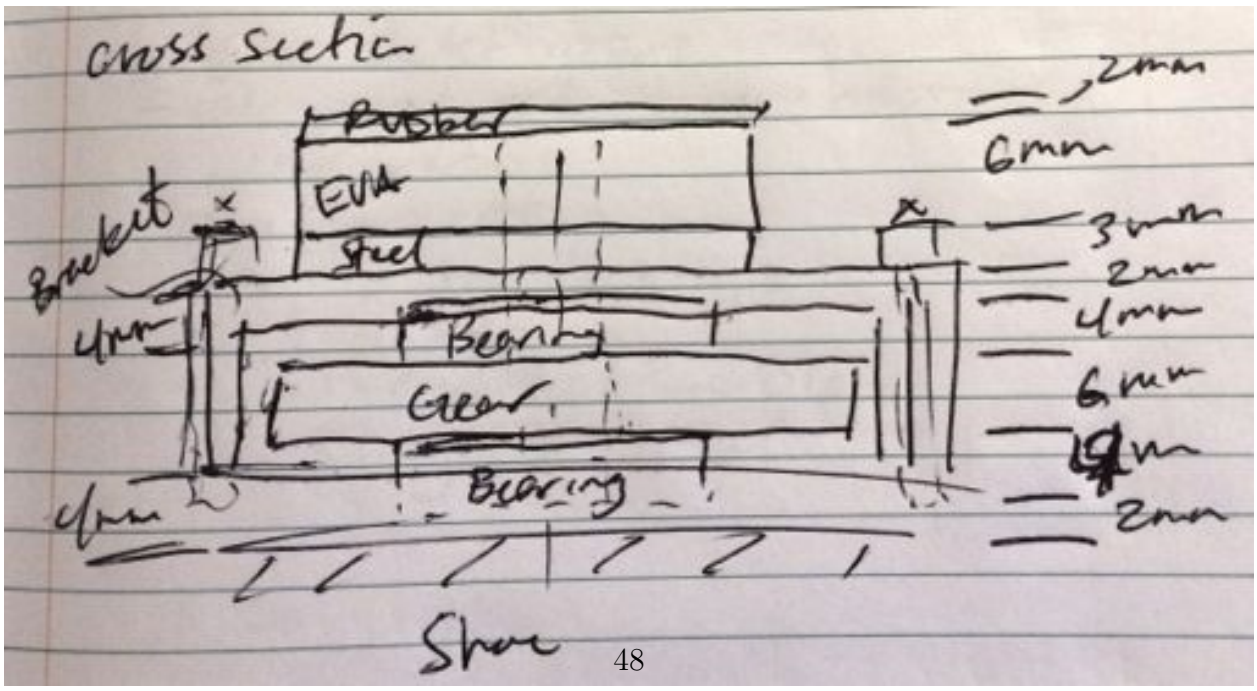

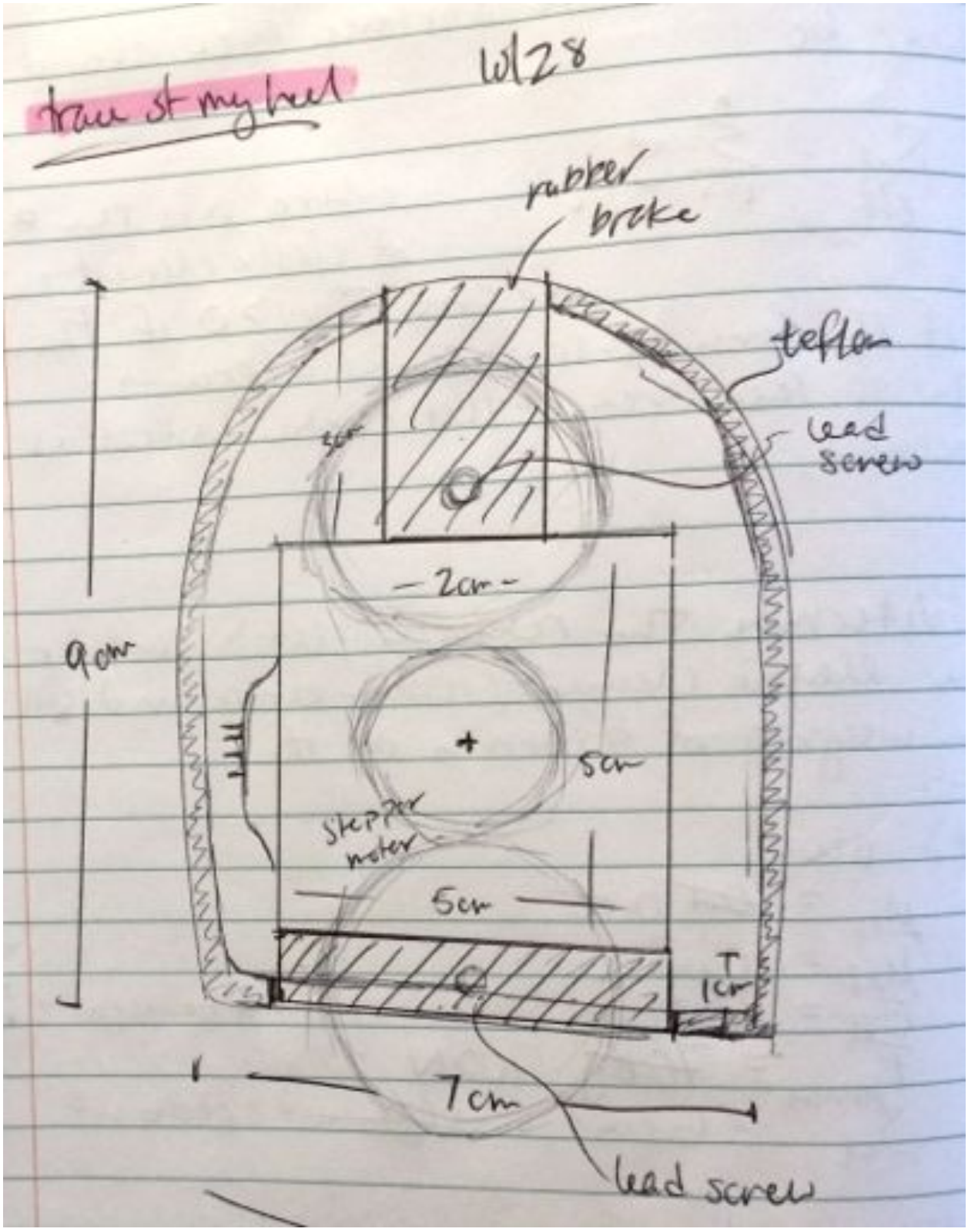


Figure D.3: Preliminary sketch of lead screw idea